Disproportionate CH_4 sink strength from an endemic, sub-alpine Australian soil microbial community

M.D. McDaniel[1,2*‡], M. Hernández[3,4*], M.G. Dumont[3,5], L.J. Ingram[1], and M.A. Adams[1,6]

1. Centre for Carbon Water and Food | Sydney Institute of Agriculture | University of Sydney | Sydney, Australia 2000
2. Department of Agronomy | Iowa State University | Ames, Iowa USA 50011
3. Max Planck Institute for Terrestrial Microbiology | Marburg, Germany D-35037
4. School of Environmental Sciences | Norwich Research Park | University of East Anglia, Norwich, UK NR4 7TJ
5. Centre for Biological Sciences | University of Southampton | Southampton, UK SO17 1BJ
6. School of Science | Engineering and Technology | The University of Swinburne | Melbourne, Australia 3122

* Co-first authors

‡ Corresponding Author:

Department of Agronomy
Iowa State University
2517 Agronomy Hall
Ames, IA 50011
Phone: (515) 294-7947
Email: marsh@iastate.edu

Running Title: Strong CH_4 uptake from unique soil microbiota

Originality-Significance Statement (about 120-150 words)

(Identify the key aspects of originality and significance that place the work within the top 10% of current research in environmental microbiology)

Novel methanotrophic bacteria have been discovered in recent years, but few studies have examined the total known diversity of methanotrophs together with the net flux of CH_4 from soils. We used an ecosystem with a vegetation-soil gradient in the sub-alpine regions of Australia (with extremely strong consumption of atmospheric CH_4) to examine microbial and abiotic drivers of CH_4 fluxes across this gradient. Recently characterized methanotrophs, either USCα in forest and grassland soils, or oxygenic *Candidatus* Methylomirabilis sp. in the bog soil were dominant. Methanotrophs belonging to the families Methylococcaceae and Methylocystaceae represented only a small minority of the methanotrophs in this ecosystem.

Abstract (200 words)

Soil-to-atmosphere methane (CH_4) fluxes are dependent on opposing microbial processes of production and consumption. Here we use a soil-vegetation gradient in an Australian sub-alpine ecosystem to examine links between composition of soil microbial communities, and the fluxes of greenhouse gases they regulate. For each soil-vegetation type (forest, grassland, and bog), we measured carbon dioxide (CO_2) and CH_4 fluxes and their production/consumption at 5-cm intervals to a depth of 30 cm. All soils were sources of CO_2, ranging from 49-93 mg CO_2 m^{-2} h^{-1}. Forest soils were strong net sinks for CH_4 at rates up to -413 µg CH_4 m^{-2} h^{-1}. Grassland soils varied with some soils acting as sources and some as sinks, but overall averaged -97 µg CH_4 m^{-2} h^{-1}. Bog soils were net sources of CH_4 (+340 µg CH_4 m^{-2} h^{-1}). Methanotrophs were dominated by USCα in forest and grassland soils, and *Candidatus* Methylomirabilis sp. in the bog soils. *Methylocystis* were also detected at relatively low abundance. The potential disproportionately large contribution of these ecosystems to global CH_4 oxidation, and poorly understood microbial community regulating it, highlight our dependence on soil ecosystem services in remote locations can be driven by a unique population of soil microbes.

Keywords: carbon dioxide; methane; 16S rRNA, methanotroph; methanogen; *Methylomirabilis*; USCalpha, *pmoA*

Introduction

Counteracting biogeochemical processes that consume or produce greenhouse gases (GHGs) regulate whether soils act as net sources or sinks. The magnitude and spatial distributions of these competing processes – whether across landscapes, with soil depth (Conrad and Rothfuss, 1991; Bender and Conrad, 1994; He *et al.*, 2012), or even within soil aggregates (Sexstone *et al.*, 1985; Ebrahimi and Or, 2016; Karbin *et al.*, 2016) – determine net release or uptake. Soils, especially upland and older soils, are nearly always sources of carbon dioxide (CO_2) to the atmosphere, owing to production of CO_2 via heterotrophic and root respiration, which overwhelm slow rates of autotrophic CO_2 consumption. On the other hand, soils can routinely be either sources or sinks for methane (CH_4) and nitrous oxide. In some cases, soils can switch from being a net source to a net sink for CH_4 and N_2O in a matter of minutes to hours (Harriss *et al.*, 1982; Wille *et al.*, 2008; McDaniel *et al.*, 2014; Hernández *et al.*, 2017). Similarly, a lateral distance of just a meter or two may result in sinks becoming sources, or vice versa (Velthof *et al.*, 1996; Priemé *et al.*, 1997; McDaniel *et al.*, 2017).

Methane is a potent greenhouse gas, 34 times as potent as CO_2, and is responsible for ~17% of anthropogenic warming (Stocker, 2013). Soil sources and sinks for CH_4 are controlled by abundance and composition of specific microbial communities (Murrell and Jetten, 2009; Nazaries, Murrell, *et al.*, 2013), but also regulated by abiotic factors (Sullivan *et al.*, 2010; Wu *et al.*, 2010; Wolf *et al.*, 2012). Oxidation of CH_4 to microbial biomass and CO_2 is, for example, restricted to distinct groups of specialized methanotrophic microorganisms. Aerobic methanotrophs belonging to the α-Proteobacteria and δ-Proteobacteria have been studied for decades and detected across a wide range of habitats (Knief, 2015). Groundbreaking research in recent years has uncovered previously uncharacterized methanotrophs, including acidophilic

Verrucomicrobia from the family Methylacidiphilaceae (Khadem *et al.*, 2012) and intra-oxygenic methanotrophs, *candidatus* Methylomirabilis oxyfera, from the NC10 phylum (Ettwig *et al.*, 2010). In addition, more recent studies have identified USCα methanotrophs, which are specialized atmospheric-CH_4 consuming bacteria whose activity has been known for decades but had evaded efforts to be isolated or characterized (Pratscher *et al.*, 2018; Singleton *et al.*, 2018; Tveit *et al.*, 2019). The first step in the biochemical pathways of CH_4 oxidation is catalyzed by the methane monooxygenase (MMO) enzyme. The *pmoA* gene encoding a subunit of the membrane-bound MMO (pMMO) enzyme is present in most aerobic methanotrophs and is frequently used as a genetic marker.

Methanogenesis in soil typically requires anaerobic and low redox conditions, with depletion of strong electronegative terminal electron acceptors, e.g. nitrate, iron. Methanogens belong to the Euryarchaeota phylum, and produce CH_4 either from CO_2 and H_2 (hydrogenotrophic methanogenesis), acetate (acetoclastic methanogenesis), or methylated single-C one-carbon compounds (Thauer et al., 2008). All known methanogenic pathways include the methyl-coenzyme M reductase enzyme encoding the *mcrA* gene, which is used as a genetic marker for methanogens in the environment. Most aerobic soils show little production of CH_4, as evidenced by low abundance of *mcrA* genes (Hernández *et al.*, 2017). A few recent studies have shown that even water-logged soil profiles tend to have an aerobic upper layer that, via its capacity for CH_4 oxidation, helps mitigate CH_4 release to the atmosphere from lower soil depths. In some cases this layer can remove 80-97% of CH_4 produced at lower depths (Conrad and Rothfuss, 1991; Frenzel *et al.*, 1992; Oremland and Culbertson, 1992; Sass *et al.*, 1992). In the field, and at ecosystem spatial scales, our understanding of the drivers of soil GHG fluxes is profoundly limited.

Local soil and vegetation gradients provide an opportunity to explore mechanisms that regulate soil GHG fluxes (Freitag *et al.*, 2010; Krause *et al.*, 2013; Christiansen *et al.*, 2016). Soil biogeochemical conditions (e.g. microbial substrates, reduction-oxidation potential, and soil pH) can vary dramatically over relatively short distances despite more-or-less constant climate. We used a forest-grassland-bog gradient located within a sub-alpine region of southern New South Wales (Fig. 1), Australia to examine the drivers of variation in soil microbial communities, and CO_2 and CH_4 fluxes. These soils are of particular interest given their previously-observed, rapid rates of CH_4 oxidation in forest and grassland soils and likely biogeochemical sensitivity to climate change. Our objective was to determine the role of soil microbial communities in regulating the production/consumption of CH_4 across this soil-vegetation gradient.

Results

Soil greenhouse gas fluxes and production at depth

Surface fluxes of CO_2 and CH_4 were measured once each season. Air temperatures ranged from 3.1 to 28.3 °C, while the average soil temperature at 0-7 cm depth was 3.6 to 16.4 (Table S1). Gravimetric water content on 17 February, when microbial community analyses were conducted, ranged from 0.25-0.79 for forest soils, 0.25-0.38 for grassland soils, and 0.9-4.66 g H_2O g dry soil^{-1} for bog soils (Table S2). The relative differences in soil temperature and moisture amongst soil-vegetation types during February extend to other three sampling dates (Table S1,S2).

Mean soil-to-atmosphere CO_2 fluxes (measured *in situ*) across the soils ranged from 2.5 to 17.4 mg CO_2 m^{-2} h^{-1}, spring and summer respectively (Fig. 2A-D). Belowground, CO_2 production (measured in the laboratory) decreased with depth. CO_2 production was

predominately from top 0-5 cm of soil, with soil means ranging from 72 to 2,357 µg CO_2 g^{-1} d^{-1}. Whereas at the 25-30 cm depth means ranged from 4 to 197 µg CO_2 g^{-1} d^{-1}. Forest and bog soils showed significantly greater CO_2 production in summer than the grassland soil at multiple depths ($P < 0.01$, Fig. 2E), ranging from 47 to 398% greater in forest soil or 60 to 282% greater in bog soil. Whereas, there were less pronounced differences amongst soil types in autumn, winter, and spring.

In situ CH_4 fluxes ranged from -413 to +778 µg CH_4 m^{-2} h^{-1} (Fig. 3A-D). Absolute fluxes, whether positive or negative, were greatest in summer compared to other seasons. Although similar pattern of soil type persisted throughout other three seasons. Forest and grassland soils mostly consumed CH_4 throughout the year (Fig. 3A-D), while bog soils were net producers of CH_4 in three of four seasons (Fig. 3A-C). Belowground, most soils (including bog) showed net CH_4 consumption at all depths to 30 cm (Fig. 3E-H). The main exception was summer where large CH_4 production of 3838 µg CO_2 g^{-1} d^{-1} was found at 5-10 cm depth ($P = 0.003$), as well as moderate production of CH_4 by all soils at 25-30 depth ranging from 87-704 µg CO_2 g^{-1} d^{-1} (Fig. 3E). The net global warming potential, measured as CO_2-equivalents, provides further evidence as the exceptional strength of the soil CH_4 sink in this ecosystem (Table 1).

Archaeal and bacterial gene abundance (qPCR) during summer (17 February 2015)

There were significant differences in archaeal 16S rRNA gene abundance between soil types, with the bog soil showing one to two orders of magnitude greater abundances than the other two soils at multiple depths ($P < 0.060$, Fig. 4A). The abundances of bacterial 16S rRNA genes were highly variable but did show a decrease with depth from 2.3×10^{11} to 1.6×10^{10} copies per g soil (Fig. 4B). There were no significant differences in abundance of bacterial 16S

rRNA genes among soil types. A *pmoA* qPCR assay targeting conventional methanotrophs belonging to the families Methylococcaceae and Methylocystaceae showed highest abundance in the bog samples (Fig 4C).

Across the soil-vegetation gradient, GHG production at depth was positively related to the soil-to-atmosphere flux of both gases (Fig. 5A, B). There was also evidence for GHG production correlating with specific gene abundances across all soil types and depths. For example, the abundance of bacterial 16S rRNA genes was linearly, positively related to CO_2 production (Fig. 5C). While, the abundance of archaeal 16S rRNA was non-linearly, positively related to CH_4 production (3-parameter exponential equation, Fig. 5D). Interestingly, however, we did not find significant relationships between abundances of archaea and CO_2, nor between bacterial abundances and CH_4.

Microbial community composition and diversity during summer (17 February 2015)

Across all soils, Illumina sequencing resulted in 440,504 archaeal, 24,293,004 bacterial, and 2,258,405 *pmoA* sequences. Both clustering and multivariate analyses (Fig. 6) show distinct differences in bacterial 16S rRNA genes between the forest/grassland and bog soils, with less forest and grassland soils being more similar. In the bog soils, *Betaproteobacteria* (OTU 1850) and OTU-1522 were more abundant than in forest and grassland soils (Fig. 6A). Contrastingly, *Rhizobiales* (OTU-78) and OTU-71 differentiated the forest/grassland from bog soils. A few OTUs were uniquely abundant in the grassland soils, like the *Chloroflexi* group (especially OTU-252, OTU-1043, OTU-249). Across multiple depths, the bog soils had greatest 16S rRNA diversity compared to the forest and grassland soils (Fig. S1). The bog soils had greater diversity, 10% and 42% larger Shannon diversity and richness (H' and S), than the average of forest and grassland soils across all depths ($P < 0.001$).

This study focused on methanotroph identification by using Illumina sequencing, of either 16S rRNA or *pmoA* genes. Both 16S rRNA and *pmoA* gene sequence data revealed that the forest and grassland soils were dominated by USCα (Figs. 7, S2) - with nearly equivalent abundances between the two soil types. The highest USCα relative abundance approached 1% of all 16S rRNA genes, and decreased with depth. *Methylocystis* were the most abundant aerobic methanotrophs detected in the bog accounting for up to 0.3% relative abundance across all depths (Fig. 7). *Candidatus* Methylomirabilis sp., which are nitrite-dependent anaerobic methanotrophs, increased with depth in the bog to a maximum of 1.5% relative abundance at 25-30 cm depths. The Illumina sequencing of the *pmoA* gene resulted in distinct differences among all three soil types, but especially between the forest/grassland and bog soils. Using *pmoA*, USCα dominated methanotroph populations in forest and grassland soils, whereas *Methylocystis* dominated bog soils (Fig. S2). Greater counts of USCα were mostly found at the surface of just one bog site (B4). This bog site has greater slope along the soil-vegetation gradient and 80-1200 % greater rock content than the other bog sites across depths (B4; Table S3, Fig 1), thus greater sand content and porosity possibly provided better habitat for methanotrophs in this bog soil.

Patterns in Community Composition and Relationships with Soil Properties

Non-metric dimensional scaling (NMDS) shows a distinct difference in bacterial 16S rRNA genes among soil types and relationship to soil properties ($P<0.05$, Fig. 6B). The communities in all soils showed a pattern with depth, but the bog soil had the most distinct separation among bacterial communities with depth. Elevated CH_4 production also correlated with depth of bog soils (Fig. 6B). The grassland soils were most positively related to clay content of the soils, and negatively with soil moisture – these were the driest of the three soil types (Fig. 6B, Table S3). The variables arguably most related to organic matter content (dissolved organic

157 and total C and N, inorganic N, and CO_2 production) correlated positively with the forest soils,
158 and the somewhat shallow bog soil depths.

159 The forest *pmoA* community was relatively tightly clustered except for one sample at 10-
160 15 cm depth (Fig. S3A). GHG production did not correlate significantly with the *pmoA*
161 community, indicating differences in the microbial community are not the direct cause of
162 production at depth. The community composition of the Euryarchaeota showed differences
163 among soil types, especially between grassland and bog soils, but no trend with depth (Fig. S3B).
164 Both GHGs and soil properties were positively related to soil organic matter, whereas clay was
165 negatively related to the bog Euryarchaeota community composition. In contrast, the community
166 composition in the grass was positively associated with soil clay content. (Fig. S3B)

167 **Discussion**

168 *Soil Microbial Community Composition and Links to Greenhouse Gas Fluxes*

169 Adjacent soils, with varying soil-forming factors (especially organisms – vegetation, and
170 landscape position) showed distinct microbial community composition and abundance with
171 depth. The bog soils tended to have the greatest abundance of archaeal 16S rRNA genes (Fig.
172 4A). At multiple depths, the bog soils also had greater diversity in bacterial and methanotroph
173 communities (Fig. 4B, C). Both of these findings are most likely due to the large total organic C
174 content in bog soils compared to the other two – when averaged across all depths, bog soils had
175 41 and 128 % greater soil organic C than the forest and grassland soils, respectively (Table S3).
176 The greater the available sources of energy (as approximated by total C) at the base of the food
177 web, the larger and more diverse we might expect the microbial communities to be (Tilman *et*
178 *al.*, 2001; Zhou *et al.*, 2002; Hartmann *et al.*, 2015).

The bog soils showed the greatest CH_4 production measured in this study at lower depths (5-10 cm, Fig. 3E), which is surprising considering that at lower depths bog soils have greater water content, i.e., likely more anoxic and methanogenic; however, this can be explained by the increasing abundance of *Candidatus* Methylomirabilis sp. with depth (Fig. 7). *Methylomirabilis* sp. are nitrite-dependent methanotrophs that oxidize CH_4 by the intracellular production of O_2 from the dismutation of NO (Ettwig *et al.*, 2010). Their presence in this habitat is consistent with previous work that suggests they are common in wetland environments (Hu *et al.*, 2014). They occur at deeper depths where nitrite is more available and exogenous O_2, which is detrimental to their activity (Luesken *et al.*, 2012). In addition, methanogenesis might be stimulated at the 5-10 cm depth by Sphagnum rhizoids that occur just above this depth (54%, Table S3). Therefore, high rhizodeposition at this depth could drive methanogenesis by supplying organic C for either acetoclastic or CO_2 reduction to CH_4 (Le Mer and Roger, 2001), coupled to relatively low CH_4 oxidation. Bog soil showed that methanogen gene expression in the top 10 cm of soil correlated linearly with the CH_4 flux, and methanotroph gene expression ratio was negatively correlated with CH_4 flux rates at a different peat bog site (Freitag *et al.*, 2010). In aggregation, microsites of CH_4 oxidation and CH_4 production, when coupled may explain the net production and strong consumption of CH_4 (Bender and Conrad, 1992, 1994; Von Fischer and Hedin, 2002; Yang and Silver, 2016).

Although not evidence of causation, patterns in soil microbial abundance and community composition were strongly related to GHG production. Given this caveat, the CO_2 production was best correlated with bacterial 16S rRNA abundance and CH_4 fluxes with archaeal 16S rRNA abundance (Fig. 5). Archaeal 16S rRNA gene abundance was best related to CH_4 production (Figs. 3E, 4C, 5E), and highlights the importance of archaeal methanogens in net CH_4

202 production (Conrad, 2002; Angel *et al.*, 2012; Nazaries, Murrell, *et al.*, 2013; Hernández *et al.*,
203 2017).

204 Methanotroph relative abundance declined with depth in the forest and grassland soil
205 (Fig. 7), similar to the findings from other studies (Bender and Conrad, 1994; Kolb *et al.*, 2005).
206 USCα methanotrophs are associated with high rates of atmospheric CH_4 oxidation in well-
207 drained habitats lacking substantial endogenous methanogenesis (Kolb *et al.*, 2005; Chen *et al.*,
208 2007; Bengtson *et al.*, 2009; Kolb, 2009; Shrestha *et al.*, 2012). The bog soils only showed CH_4
209 consumption at the 0-5 cm depth during the summer when soil-to-atmosphere CH_4 fluxes were
210 highest (Fig. 3A, 3E), which corresponded to the soil depth the greatest proportion of USCα (Fig
211 7, S2). Thus, USCα abundance, greater O_2 availability, and lower methanogenesis in the top 0-5
212 cm all could contribute to the high capacity for aerobic CH_4 oxidation at the surface of bog soils.
213 Although *Candidatus* Methylomirabilis were highly abundant at depth, their per-cell CH_4
214 oxidation capacity might be lower than for aerobic methanotrophs (Luesken *et al.*, 2012).
215 Furthermore, the activity of *Candidatus* Methylomirabilis might have been inhibited by O_2
216 exposure during the subsectioning of the cores. Finally, although aerobic methanotrophs can
217 survive in low O_2 environments, in part by energy generation via fermentation reactions
218 (Kalyuzhnaya *et al.*, 2013; Kits *et al.*, 2015), the rates of CH_4 oxidation will be lower than most
219 well-oxygenated surface soils.

220 The three soils had distinct microbial community compositions, with the forest and
221 grassland soils being the most similar (Fig. 6, 7, S2, S3). The bog soils had greater abundances
222 of bacterial 16S rRNA OTU in the family *Ktedonobacterales* (OTU-1522) and an unclassified
223 *Betaproteobacteria* (OTU 1850, Fig. 6A). All soils showed a pattern with depth, but the bog
224 soils showed the greatest discrimination with depth (Fig. 6B). Some microorganisms in the

225 *Ktedonobacterales* have been cultured, and these are Gram-positive, aerobic, broad temperature
226 ranges (meso- to thermophilic), and are characterized by having multicellular filaments and
227 spores – similar to actinomycetes (Yokota, 2012; Yabe *et al.*, 2017). The unclassified
228 *Betaproteobacteria* are likely ammonia-oxidizing bacteria and did not play a significant role in
229 CH_4 oxidation (Bodelier and Frenzel, 1999). The forest soils showed greater abundance of an
230 unclassified *Gammaproteobacteria*, which could potentially be either methanotrophic or
231 ammonia-oxidizing bacteria.

232 Within the methanotroph community, the bog soils showed a distinctly greater abundance
233 of *Methylocystis* spp., *Ca*. Methylomirabilis, and unclassified proteobacterial methanotrophs (Fig
234 7 and S2). *Methylocystis* typically proliferate at CH_4 concentrations > 40ppm, which would
235 occur in bog soils where concentrations (and production) of CH_4 are greatest. A recent study
236 showed this is indeed the case where low-affinity methanotroph activity is dependent on high
237 supply of CH_4, and may trigger high-affinity activity during drought (Cai *et al.*, 2016). The
238 grassland and forest soils were predominately composed of *Methylocystis* and USCα (Fig 7 and
239 S2). The USCα, are classified as high-affinity, with apparent K_m values of 0.01-0.28, compared
240 to that of 0.8-32 for low-affinity methanotrophs (Shukla *et al.*, 2013). Several studies now
241 confirm that forest or grassland soils that have high CH_4 oxidation potential also have high
242 abundance of *Methylocystis* or USCα methanotrophs (Knief *et al.*, 2003; Malghani *et al.*, 2016).
243 There is mounting evidence, including this study, that indicate the absence/presence of specific
244 methanotrophic bacteria or methanotrophic community composition might be just as important
245 as physicochemical regulators on net CH_4 fluxes from soils (Nazaries *et al.*, 2011; Nazaries, Pan,
246 *et al.*, 2013; Malghani *et al.*, 2016). Other studies show CH_4 fluxes are largely regulated by
247 physical processes such as substrate diffusion (Saari *et al.*, 1997; Wille *et al.*, 2008; Fest *et al.*,

248 2015; D'imperio *et al.*, 2017) or labile C supply (Pratscher *et al.*, 2011; Sullivan *et al.*, 2013);
249 however, due to the high sensitivity of methanotrophic bacteria to physicochemical conditions it
250 is difficult to tease these factors apart (Nazaries *et al.*, 2011; Fest *et al.*, 2015).

251 Our study and others (Conrad and Rothfuss, 1991; Frenzel *et al.*, 1992) show that surface
252 soils even in consistently wet soils (0-5 cm, Fig. 3) can be a sink not only for atmospheric CH_4,
253 but also a likely filter for CH_4 produced at greater depths (Cai *et al.*, 2016). Given that by some
254 estimates as much as 80-97% of endogenously produced CH_4 at depth is consumed before
255 reaching the atmosphere (Conrad and Rothfuss, 1991; Frenzel *et al.*, 1992; Oremland and
256 Culbertson, 1992; Sass *et al.*, 1992), the disturbance of this thin layer of soil could result in
257 larger net CH_4 fluxes as CH_4 produced at depth diffuses toward the atmosphere and is not
258 oxidized in this surface layer. The complex dynamics, high net CH_4 uptake rates of the forest
259 and grassland soils (Fig. 9A), and high consumption at the surface of the bog soils are all reasons
260 why it is crucial to understand the microbial mechanisms driving these greenhouse gas fluxes.

261

262 *Australian Alps: Unique Soils with Disproportionate CH_4 Sink Strength*

263 Across the globe, aerated upland soils provide a net CH_4 sink that ranges from 7-100 Tg
264 y^{-1} (Smith *et al.*, 2000), which is estimated to be up to 15% of the total global CH_4 sink
265 (Reeburgh, 2003; Dutaur and Verchot, 2007; Shukla *et al.*, 2013). The Australian Alps are
266 restricted to the southeastern corner of the mainland totaling 0.16% of Australia's area (Fig. 8).
267 We studied 538 ha of a 1.2M ha region, but found convincing evidence for the overwhelming
268 CH_4 sink strength of this region's soils (Fig. 9A).

We used a combination of foliar coverage estimates for extrapolation across the region, climate station data to interpolate CH_4 fluxes between seasonal measurements, and range in global sink strength from the literature (Table 2), to parameterize the disproportionate contribution of this endemic ecosystem to the global soil CH_4 sink. While only comprising <0.03% of global forested and grassland ecosystems, this unique Australian ecosystem could represent 6 up to >100% of global soil methane sink (Kirschke *et al.*, 2013; Saunois *et al.*, 2016). While it is unreasonable to expect these unique soils to make up more than 100% of the global CH_4 sink, it illustrates the problem with the low estimates for the global soil CH_4 sink (Kirschke *et al.*, 2013; Saunois *et al.*, 2016; Gatica *et al.*, 2020). These soils are undoubtedly amongst the greatest negative CH_4 fluxes observed at an hourly scale (Fig. 9A), and our data conform to other annual CH_4 flux estimates despite the acknowledged error of these estimates with so few observations (Gatica *et al.*, 2020; Fig. 9B). Monitoring CH_4 fluxes at high spatial and temporal resolution in remote locations remains a major challenge.

Soils under all three vegetation types were sources of CO_2 with positive GWPs, yet ranged from strong negative to positive GWP contributions from CH_4 (Table 1). The CH_4 sink under grassland and forest soils provided 53% and 56% GWP offset (in negative CO_2-equivalents) of the net CO_2 emissions respectively. All soils consumed CH_4 at 0-5 cm depth. This is consistent with other studies showing high uptake in surface soils where O_2 is more available (Koschorreck and Conrad, 1993; Bender and Conrad, 1994; Hütsch, 1998), even lake sediments can show similar CH_4 oxidation profiles with depth (He *et al.*, 2012). However, many studies find maximum oxidation rates are not near the soil surface, but 5-10 cm below (Bender and Conrad, 1994; Hütsch *et al.*, 1994; Schnell and King, 1994; Priemé and Christensen, 1997; Wolf *et al.*, 2012). Differences in where this maximum CH_4 consumption depth occurring are

dependent on soil texture, organic matter content, and moisture content with depth along with substrates that are also thought to regulate CH_4 oxidation like labile C or inorganic N that are also more available in surface soils (Priemé and Christensen, 1997; Pratscher *et al.*, 2011; Sullivan *et al.*, 2013).

This endemic ecosystem, with an arguably disproportionate importance to the global soil CH_4 sink (Tables 1,2; Fig. 8), are amongst the ecosystems most likely to be affected by changes in climate, as was recently demonstrated by declines in CH_4 uptake in several long-term studies of forest soils (Ni and Groffman, 2018). More frequent and intense forest fires are just one global change threat to these Australian Alps soils (Adams, 2013; Adams *et al.*, 2013), with potential positive feedbacks to climate change. We are increasingly reliant on key soil ecosystem services to thrive on planet Earth (Jónsson and Davíðsdóttir, 2016), and agroecosystem soils get much of the attention due to proximal benefits (i.e. crop production). Global soil ecosystem services, however, like that of strong atmospheric CH_4 oxidation occurring in these Australian Alps soils, are not as obvious nor as easy to value but critical for buffering against anthropogenic climate change.

Experimental Procedures

Study Site Characteristics

Our study sites were located in an area known locally as the Snowy Plains, within the Snowy Mountains region of southern New South Wales. The Snowy Plains are form part of the Australian Alps montane grasslands, and lie adjacent to the Kosciuszko National Park (36º10′ S, 148º54 ′E; Fig. 1). The elevation range of the sampling area within the Snowy Plains was 1471

to 1677 masl. The mean annual temperature and precipitation are 6.4 ºC and ~1600 mm (SILO - Queensland Government). The site remains snow-covered typically for 2-3 months of the year.

The area is a mosaic ecosystem containing a mixture of bog, grassland, and forest (Fig. 1) and has been well described elsewhere (e.g. Jenkins and Adams, 2010). Alpine humus soils (Chernic tenosol) in the region are ~400 million years old and derived from glacial moraines of Silurian Mowomba granodiorite (Costin *et al.*, 1952). They show little horizon development in the top 30 cm (Fig. S4). Soil are mostly sandy loams in texture, and pH ranges from ~5.3-5.7 down to 30 cm, across all sites (Table S3). Bogs are dominated by *Sphagnum spp.* and some sparse grass cover (*Poa spp*). Grasslands are dominated mostly by *Poa hiemata* and *Poa costiniana*. Forests are dominated by Snow Gums (*Eucalyptus pauciflora*), with the N-fixing shrub *Bossiaea foliosa*, and some *Poa* spp. as understory and ground layers.

Experimental Design, Soil Sampling, and Gas Sampling

We used four topographic transects (from bogs and grasslands in the lowest part of the landscape, to forests in upland areas) to guide our soil and GHG sampling (Fig. 1). After each sampling location was determined, a 15-cm diameter (5-cm deep) PVC collar was installed for soil GHG sampling a minimum of 1 month prior to sampling, in order to preclude artifacts introduced by recent disturbance. We measured greenhouse gas fluxes *in situ* and collected soils on 17 February, 25 May, 22 September, and 23 November in 2015. But in-depth microbial sampling and analyses were conducted only on soils collected on 17 February – the time of year for peak CH_4 production and consumption.

GHG fluxes were measured *in situ* using the static chamber method. We first placed a 3.2 L, vented, PVC chamber over the collar. Four gas samples were collected every 10-15 minutes and directly injected into a Labco Exetainer vial. Concurrent measurements of soil

337 moisture (Theta Probe, Delta-T DevicesTheta Probe, Cambridge, UK) and temperature (Novel
338 Ways, Hamilton, NZ) were taken in triplicate and averaged for each measurement location (7 cm
339 depth).

340 Immediately after completing gas sampling, the chambers were removed, and a 5-cm
341 diameter 30-cm deep soil core was taken directly in the center of the collar. These cores were
342 used for determination of soil properties, microbial community analyses, and to measure net CO_2
343 production and CH_4 production/consumption in the laboratory. The 30-cm soil cores were
344 stratified and dissected in the field with a clean knife at 5-cm intervals. At each depth, a
345 subsample (~ 3-5 g of soil) was immediately placed into a 2-ml Eppendorf tube, then placed in
346 liquid nitrogen and stored at -80 °C until DNA was extracted. The remainder of the soil core
347 was placed in a protective PVC sleeve, and then stored in an iced cooler until reaching the
348 laboratory.

349 Soil cores from the field were transferred to 1 L jars where they were briefly incubated at
350 near-ambient air temperature at the time of collection (22 °C) in order to further characterize
351 CO_2 and CH_4 production and consumption occurring at each depth (*sensu* Bender and Conrad,
352 1994). This procedure has been found to be highly related ($r^2 = 0.44$, n = 30) to *in situ* CH_4
353 production/consumption (Priemé and Christensen, 1997). The incubations began by placing the
354 relatively undisturbed soil cores into the jars, flushing them with ambient air, and then placing
355 the lids on the jars. The lids had Luer-lock access, and four gas samples were taken over the
356 short-term (3-day) incubations and placed directly into Labco Exetainer vials. Once the
357 incubations finished, the soils were air dried for physical and chemical analyses. The GHG
358 concentrations were analyzed on a gas chromatograph.

359 *Soil Processing and Analyses*

360 Soils were sieved (2 mm) and both rocks and roots were removed and weighed. A sub-
361 sample was ground for total C and N analysis on a TruSpec Elemental Analyzer (LECO, St.
362 Joseph, MI, USA). Soil texture was analyzed by using the hydrometer method (Gee and Bauder,
363 1986). Soil inorganic N (ammonium and nitrate) was measured by extracting 5 g of soil with 40
364 ml of 0.5 M K_2SO_4 shaken for 1 h and filtered with Whatman #1. These extracts were analyzed
365 on a Lachat Injection-flow Analyzer according to standard methods (Lachat Instruments,
366 Loveland, CO, USA). Dissolved organic C and N were analyzed on the same extracts on a
367 Shimadzu TOC-N Analyzer (Shimadzu Scientific Instruments Inc., Columbia, MD, USA).
368 Electrical conductivity and pH were measured on SevenMulti probe (MettlerToledo, Columbus,
369 OH, USA) with a 1:1 (w:w) ratio with de-ionized water. Heavy elements were analyzed by X-
370 ray fluorescence using a Niton XL3 t Ultra Analyzer meter (Thermo Scientific, Waltham, MA,
371 USA).

372 *DNA Extraction and Quantitative PCR*

373 Total DNA was extracted using the NucleoSpin® Soil kit (Macherey-Nagel, Germany) by
374 disrupting the cells by bead beating (30 s at 5.5 m s^{-1}). DNA purity and quantification were
375 determined using a NanoDrop® Spectrophotomoter ND-1000 (Thermo Fisher Scientific, USA).
376 DNA at a concentration of 10 ng μl^{-1} was stored at -20 °C for further molecular analysis. The
377 abundance of bacterial- and archaeal- 16S rRNA genes as well as *pmoA* genes was performed
378 using an iCycler Instrument (BioRad). For all assays, standards containing known number of
379 DNA copies of the target gene were used. qPCR conditions for archaeal- and bacterial- 16S
380 rRNA genes were based on dual-labeled probes. For bacterial 16S rRNA genes, primers
381 Bac338F, Bac805R and Bac516P were used. For archaeal 16S rRNA genes, primers Arc 787F,

382 Arc1059R and Arc915P were used. Conditions for both genes were as follows: 0.5 µM of each
383 primer, 0.2 µM of the dual-labeled probe, 3 µl of template, 4 mM $MgCl_2$ (Sigma) and 12.5 µl of
384 JumpStart Ready Mix (Sigma-Aldrich). 1 µl of BSA (0.8 µg/µl) was added to archaeal 16S
385 rRNA gene reactions. The program used for both assays was 94 °C for 5 min, 35 cycles of 95 °C
386 for 30 s and 62 °C for 60 s extension and signal reading (Yu *et al.*, 2005). qPCR condition for
387 *pmoA* genes was using SYBR Green (Sigma-Aldrich) and primers A189F / mb661R. PCR
388 conditions were 0.667 µM of each primer, 3 µl template, 4 mM $MgCl_2$ (Sigma), 0.25 µl FITC
389 (1:1000), 12.5 µl of SYBR Green JumpStart *Taq* Ready Mix (Sigma-Aldrich) and 0.6 µl of BSA
390 (0.5 µg/µl). PCR program was 94 °C for 6 min, followed by 45 cycles of 94 °C for 25 s, 65.5 °C
391 20 s, 72°C 35s, 72°C 10 s plate read. The final melting curve was as follows: 100 cycles of 75-
392 94.8°C 6s, +0.2 °C $cycle^{-1}$ (Kolb *et al.*, 2003). Efficiencies of 99.6% for bacterial 16S rRNA
393 genes, 78.8 – 84.9% for archaeal 16S rRNA genes, and 77.2 – 78.5% for *pmoA* genes were
394 obtained, all with R^2 values > 0.99. Technical duplicates were performed for each of the
395 replicates.

396 *Illumina library preparation and sequencing*

397 MiSeq Illumina sequencing was performed for total 16S rRNA and *pmoA* genes. PCR
398 primers 515F / 806R targeting the V4 region of the 16S rRNA gene (approximately 250
399 nucleotides) were used (Bates *et al.*, 2011) with an initial denaturation at 94 °C for 5 min,
400 followed by 28 cycles of 94 °C for 30 s, 50 °C for 30 s, and 68 °C for 30 s and a final elongation
401 at 68 °C for 10 min (Hernández *et al.*, 2015). The amplification of *pmoA* genes was performed
402 via a semi-nested PCR approach using the primers A189F/A682R for the first round PCR
403 (Holmes *et al.*, 1995) as follows: 94 °C for 3 min followed by 30 cycles of 94 °C 45 s, 62 to 52
404 °C (touchdown 1 °C per cycle) for 60 s, 68 °C 3 min, and a final elongation of 68 °C 10 min

(Horz *et al.*, 2005). Aliquots of the first round of PCR (0.5 µl) were used as the template in the second round of PCR using the primers A189f / A650r / mb661r in a multiplex PCR as follows: 94 °C for 3 min followed by 25 cycles of 94 °C 45 s, 56 °C 60 s and 68°C 1 min, and final elongation of 68 °C 10 min (Horz *et al.*, 2005). Individual PCRs contained a 6-bp molecular barcode integrated in the forward primer. Amplicons were purified using a PCR cleanup kit (Sigma) and quantified using a Qubit 2.0 fluorometer (Invitrogen). An equimolar concentration of the samples was pooled for each of the genes and sequenced on separate runs using 2 x 300 bp MiSeq paired-end protocol. Library preparation and sequencing was performed at the Max Planck Genome Centre (MPGC), Cologne, Germany. Table S4 summarizes primer sequences for both genes and barcode sequences for each of the samples.

Bioinformatics, Data processing, GIS modeling, and Statistical Analyses

For 16S rRNA genes, quality filtering and trimming forward and reverse adaptors from the sequences was carried out using the tool cutadapt (Martin, 2011). Forward and reverse reads were merged using the usearch fastq_mergepairs command (Edgar, 2013). For the *pmoA* gene, one-end run was performed, and the forward adaptor was trimmed using cutadapt. Downstream processing was performed with UPARSE (Edgar, 2013) and UCHIME pipelines (Edgar *et al.*, 2011) following the steps detailed in Reim et al. (Reim *et al.*, 2017). For 16S rRNA genes, a representative sequence of each operational taxonomic unit (OTU) was classified based on the SILVA-132 16S rRNA gene database using the naïve Bayesian classifier (bootstrap confidence threshold of 80%) in mothur (Schloss *et al.*, 2009). The *pmoA* genes were classified using the same method, but using the *pmoA* database (Dumont *et al.*, 2014). Sequence data were deposited in the NCBI Sequence Read Archive (SRA) under accession number PRJNA384296.

A USCα 16S rRNA gene sequence has recently been identified (Pratscher *et al.*, 2018), which enabled us to search these sequences in our dataset. The 16S rRNA genes were identified by standalone BLAST against the 16S rRNA OTUs using the USCa_MF sequence (Genbank ID MG203879). Those OTUs with percent ID > 98% relative to the USCa_MF were positively identified as USCα. The relative abundance of USCα in each of the samples could then be calculated from the OTU table.

Greenhouse gas fluxes (both field and incubation) were calculated using a linear regression, or change in the GHG over the time between gas samples. Data was screened for normality and heterogeneity of variances, and when not conforming was log-transformed (Zuur *et al.*, 2010) for statistical analyses (all CO_2 and gene abundance data). All univariate statistics were conducted in SAS (v. 9.4). Comparisons of variance among soil/vegetation types (bog, grassland, forest) were completed using 1-way ANOVA ($\alpha = 0.05$) with transect considered random, and depth not included in interactions since depth effects are not independent. Post-hoc tests were completed using lsmeans, adjusted using Tukey's for multiple comparisons. Multivariate statistics for 16S rRNA Illumina data was analyzed by using the vegan package (Oksanen *et al.*, 2016) in R software version 3.0.1 (R Core Team, 2018). Non-metric multidimensional scaling (NMDS) was performed using the *decostand* function for ordination of Hellinger distances. Influence of environmental variables on the total diversity of 16S rRNA and *pmoA* genes was analyzed by the *envfit* function (vegan package in R, permutations = 999). Heatmaps were constructed with the gplots package (Warnes *et al.*, 2015). Principal components analysis (PCA) of the Hellinger transformed data was performed using the prcomp function. The OTUs explaining most of the differences between samples were defined as the 10 OTUs contributing the largest absolute loadings in the first and second dimensions of the PCA,

obtained from the rotation output file (Hernández *et al.*, 2017). Hierarchical clustering of the distance matrix used the "ward.D2" method and *hclust* function. The heatmap was constructed using the *heatmap.2* function in *ggplots* package (Hernández *et al.*, 2017).

Using the four field-measured, hourly CH_4 fluxes we developed a model to estimate annual CH_4 production across the Australian Alps based on number of geographic information system (GIS) datasets. The datasets included elevation and aspect (30 m pixel) as well as daily estimates of maximum and minimum air temperature (BOM, 2020) and soil moisture (0 – 0.1 m; Frost *et al.*, 2018). The climate data rasters were all a 5 km pixel size. For each of the days for that CH4 fluxes were determined in the field, the location of 12 sites was used to extract data from each of the raster datasets using ArcGIS (V10.8, ESRI Systems, CA). This data was then used to develop a linear regression model using R (v 4.0.2). The final linear regression model (p-value = <0.0001, F-statistic = 14.95, adjusted r2 = 0.77) included the main factors (the ecosystem measured; Bog, Forest & Grassland) along soil moisture and maximum air temperature and interactions. The spatial extent of each ecosystem across the Australian Alps bioregion (IBRA7, 2012) was based on tree cover in 2015 (DEE, 2018); Forest sites were located in >20% projected foliage cover and Grassland sites <20% projected foliage cover and the Bog sites were considered to be within 1 m of a hydrological flow surface developed using the TauDEM ArcGIS toolset (v5.3.7; Tarboton, 2005). This data along with average seasonal estimates of maximum air temperature and soil moisture were then computed for the Australian Alps. In small number of cases, individual pixels of the maximum air temperature and soil moisture rasters exceeded the maximum/minimum points on which the linear regression model had been developed, in which case they were forced to the maximum/minimum value. The linear

472 regression previously developed was then used to predict seasonal estimate of CH_4 fluxes for
473 each of the ecosystems measured across the Australian Alps.

474

475 **Acknowledgements**

476 Funding for this research was provided by an anonymous donor. Prof. Dr. Ralf Conrad,
477 at the Max Planck Institute in Marburg, Germany, provided facilities and advice. We would like
478 to kindly thank Barry Aitchison, whom provided us with site access and a wonderful cabin to
479 spend the evenings around the fire. Hero Tahai assisted with laboratory procedures.

480

481 **Table legends**

482 **Table 1**. Annual estimates (mean, standard error, and range) for net ecosystem flux of carbon

483 dioxide and methane

484 **Table 2**. Comparison of Global and Australian Alps soil methane sink estimates

485

Figure legends

Figure 1. A) Location of 548 ha experiment area (inset of Australia), sampling sites within area and nearby streams. B) Landscape-level photograph of the vegetation gradient from sphagnum-dominated bog in foreground to eucalyptus-dominated forest in background. Abbreviations are F = Forest, G = Grassland, and B = Bog. The numbers after the letter represent which transect the sampling location belongs to.

Figure 2. Soil CO2 fluxes (top panels, A-D) and production (bottom panels, E-H). Surface flux measurements and soils collected for production on 17 February (Summer,A & E), 25 May (Autumn, B & F), 22 September (Winter, C & G), and 23 November (Spring, D & H) in 2015. Mean and standard error shown (n = 4).

Figure 3. Soil CH4 fluxes (top panels, A-D) and production/consumption (bottom panels, E-H). Surface flux measurements and soils collected for production on 17 February (Summer,A & E), 25 May (Autumn, B & F), 22 September (Winter, C & G), and 23 November (Spring, D & H) in 2015. Mean and standard error shown (n = 4).

Figure 4. Abundance of archaeal (A) and bacterial (B) 16S rRNA genes, and pmoA (C). Means and standard error are shown (n=4) for all samples.

Figure 5. Regressions between total CO2 production and CO2 soil-atmosphere flux (A), CH4 production and CH4 soil-atmosphere flux (B). Total GHG production was calculated for each soil profile as sum of production from 0 to 30 cm depth. Regressions between bacterial 16S rRNA abundance with CO2 production (C, linear equation with log, log scale). Regression between and archaeal 16S rRNA and CH4 production (D, 3-parameter exponential, log x-axis). Equations, chosen by best fit, are shown in each panel.

Figure 6. A) Heatmap of the most relevant OTUs derived from bacterial 16S rRNA genes. The samples and OTUs were clustered according to Euclidean distances between all Hellinger transformed data. The taxonomy of OTUs was determined using the Sina classifier. The colored scale gives the percentage abundance of OTUs. B) NMDS ordination of bacterial 16S rRNA communities based on the Bray–Curtis dissimilarity of community composition (stress =0.061). Arrows indicate the direction at which the environmental vectors fit the best (using the envfit function) onto the NMDS ordination space. EC, electrical conductivity; DOC, dissolved organic carbon; DON, dissolved organic nitrogen; GWC, gravimetric water content.

Figure 7. Relative abundance of 16S rRNA genes of the dominant methanotroph groups detected in the forest (A), grass (B), and bog (C) sites. USCα was identified by blast as described in the methods. Methylocystis and Methylomirabilis were identified based on the Silva classifications. Other methanotrophs include Methylomonas and Methylospira.

Figure 8. Areal coverage of Australian Alps in southeastern Australia (1.2M ha).

Figure 9. A) Hourly methane (CH_4) fluxes from this study's Forest, Grassland and Bog soils compared to Forest and Herbaceous studies from a global meta-analysis (McDaniel et al. 2019). 10^{th} and 90^{th} percentile shown by bottom and top whisker. 25^{th} and 75^{th} percentile shown by bottom and top of the box. Median is shown by the thin line, mean by the thick line, and outliers are circles. The number of measurements within each boxplot are shown in parentheses. Gray bar at -571 μg CH_4 m^{-2} h^{-1} is the greatest CH4 oxidation rate (most negative flux) ever observed and published (Singh *et al.*, 1997). B) Figure from survey of global forest CH4 fluxes (Gatica *et al.*, 2020) with our modeled annual mean net CH4 sink from Australian Alps and range created ± relative standard deviation from ecosystem means (Table 2).

REFERENCES

Adams, M.A. (2013) Mega-fires, tipping points and ecosystem services: Managing forests and woodlands in an uncertain future. *For Ecol Manage* **294**: 250–261.

Adams, M.A., Cunningham, S.C., and Taranto, M.T. (2013) A critical review of the science underpinning fire management in the high altitude ecosystems of south-eastern Australia. *For Ecol Manage* **294**: 225–237.

Angel, R., Claus, P., and Conrad, R. (2012) Methanogenic archaea are globally ubiquitous in aerated soils and become active under wet anoxic conditions. *ISME J* **6**: 847–862.

Bates, S.T., Cropsey, G.W.G., Caporaso, J.G., Knight, R., and Fierer, N. (2011) Bacterial communities associated with the lichen symbiosis. *Appl Environ Microbiol* **77**: 1309–1314.

Bender, M. and Conrad, R. (1992) Kinetics of CH4 oxidation in oxic soils exposed to ambient air or high CH4 mixing ratios. *FEMS Microbiol Lett* **101**: 261–269.

Bender, M. and Conrad, R. (1994) Methane oxidation activity in various soils and freshwater sediments: Occurrence, characteristics, vertical profiles, and distribution on grain size fractions. *J Geophys Res Atmos* **99**: 16531–16540.

Bengtson, P., Basiliko, N., Dumont, M.G., Hills, M., Murrell, J.C., Roy, R., and Grayston, S.J. (2009) Links between methanotroph community composition and CH4 oxidation in a pine forest soil. *FEMS Microbiol Ecol* **70**: 356–366.

Bodelier, P.L.E. and Frenzel, P. (1999) Contribution of methanotrophic and nitrifying bacteria to CH4 and NH4 + oxidation in the rhizosphere of rice plants as determined by new methods of discrimination. *Appl Environ Microbiol* **65**: 1826–1833.

551 BOM (2020) Bureau of Meteorology. Maps. Recent and Past Conditions.

552 Cai, Y., Zheng, Y., Bodelier, P.L.E., Conrad, R., and Jia, Z. (2016) Conventional methanotrophs
553 are responsible for atmospheric methane oxidation in paddy soils. *Nat Commun* **7**:.

554 Chen, Y., Dumont, M.G., Cébron, A., and Murrell, J.C. (2007) Identification of active
555 methanotrophs in a landfill cover soil through detection of expression of 16S rRNA and
556 functional genes. *Environ Microbiol* **9**: 2855–2869.

557 Christiansen, J.R., Levy-Booth, D., Prescott, C.E., and Grayston, S.J. (2016) Microbial and
558 Environmental Controls of Methane Fluxes Along a Soil Moisture Gradient in a Pacific
559 Coastal Temperate Rainforest. *Ecosystems* **19**: 1255–1270.

560 Conrad, R. (2002) Control of microbial methane production in wetland rice fields. *Nutr Cycl*
561 *Agroecosystems* **64**: 59–69.

562 Conrad, R. and Rothfuss, F. (1991) Methane oxidation in the soil surface layer of a flooded rice
563 field and the effect of ammonium. *Biol Fertil Soils* **12**: 28–32.

564 Costin, A.B., Hallsworth, E.G., and Woof, M. (1952) Studies in pedogenesis in New South
565 Wales. *J Soil Sci* **3**: 190–218.

566 D'imperio, L., Nielsen, C.S., Westergaard-Nielsen, A., Michelsen, A., and Elberling, B. (2017)
567 Methane oxidation in contrasting soil types: responses to experimental warming with
568 implication for landscape-integrated CH4 budget. *Glob Chang Biol* **23**: 966–976.

569 DEE (2018) Department of Energy and Environment. Woody Cover National Forest and Sparse
570 Woody Vegetation Data (Version 3).

571 Dumont, M.G., McGenity, T.J., Timmis, K.N., and Nogales, B. (2014) Primers: functional

572 marker genes for methylotrophs and methanotrophs. *Hydrocarb Lipid Microbiol Protoc eds*
573 *McGenity TJ, Timmis KN, Nogales B, Ed Springer-Verlag* 1–21.

574 Dutaur, L. and Verchot, L. V (2007) A global inventory of the soil CH4 sink. *Global*
575 *Biogeochem Cycles* **21**: 1–9.

576 Ebrahimi, A. and Or, D. (2016) Microbial community dynamics in soil aggregates shape
577 biogeochemical gas fluxes from soil profiles – upscaling an aggregate biophysical model.
578 *Glob Chang Biol* **22**: 3141–3156.

579 Edgar, R.C. (2013) UPARSE: highly accurate OTU sequences from microbial amplicon reads.
580 *Nat Methods* **10**: 996.

581 Edgar, R.C., Haas, B.J., Clemente, J.C., Quince, C., and Knight, R. (2011) UCHIME improves
582 sensitivity and speed of chimera detection. *Bioinformatics* **27**: 2194–2200.

583 Ettwig, K.F., Butler, M.K., Le Paslier, D., Pelletier, E., Mangenot, S., Kuypers, M.M.M., et al.
584 (2010) Nitrite-driven anaerobic methane oxidation by oxygenic bacteria. *Nature* **464**: 543–
585 548.

586 Fest, B., Wardlaw, T., Livesley, S.J., Duff, T.J., and Arndt, S.K. (2015) Changes in soil moisture
587 drive soil methane uptake along a fire regeneration chronosequence in a eucalypt forest
588 landscape. *Glob Chang Biol* **21**: 4250–4264.

589 Von Fischer, J.C. and Hedin, L.O. (2002) Separating methane production and consumption with
590 a field-based isotope pool dilution technique. *Global Biogeochem Cycles* **16**: 1–13.

591 Freitag, T.E., Toet, S., Ineson, P., and Prosser, J.I. (2010) Links between methane flux and
592 transcriptional activities of methanogens and methane oxidizers in a blanket peat bog.

FEMS Microbiol Ecol **73**: 157–165.

Frenzel, P., Rothfuss, F., and Conrad, R. (1992) Oxygen profiles and methane turnover in a flooded rice microcosm. *Biol Fertil Soils* **14**: 84–89.

Frost, A.J., Ramchurn, A., and Smith, A. (2018) The Australian Landscape Water Balance model.

Gatica, G., Fernández, M.E., Juliarena, M.P., and Gyenge, J. (2020) Environmental and anthropogenic drivers of soil methane fluxes in forests: Global patterns and among-biomes differences. *Glob Chang Biol* **26**: 6604–6615.

Gee, G.W. and Bauder, J.W. (1986) Particle-size analysis. In *Methods of soil analysis: Part 1—Physical and mineralogical methods*. Soil Science Society of America, American Society of Agronomy, pp. 383–411.

Harriss, R.C., Sebacher, D.I., and Day, F.P. (1982) Methane flux in the Great Dismal Swamp. *Nature* **297**: 673–674.

Hartmann, M., Frey, B., Mayer, J., Mäder, P., and Widmer, F. (2015) Distinct soil microbial diversity under long-term organic and conventional farming. *ISME J* **9**: 1177–1194.

He, R., Wooller, M.J., Pohlman, J.W., Quensen, J., Tiedje, J.M., and Leigh, M.B. (2012) Diversity of active aerobic methanotrophs along depth profiles of arctic and subarctic lake water column and sediments. *ISME J* **6**: 1937–1948.

Hernández, M., Conrad, R., Klose, M., Ma, K., and Lu, Y. (2017) Structure and function of methanogenic microbial communities in soils from flooded rice and upland soybean fields from Sanjiang plain, NE China. *Soil Biol Biochem* **105**: 81–91.

614 Hernández, M., Dumont, M.G., Yuan, Q., and Conrad, R. (2015) Different bacterial populations
615 associated with the roots and rhizosphere of rice incorporate plant-derived carbon. *Appl*
616 *Environ Microbiol* **81**: 2244–2253.

617 Holmes, A.J., Costello, A., Lidstrom, M.E., and Murrell, J.C. (1995) Evidence that participate
618 methane monooxygenase and ammonia monooxygenase may be evolutionarily related.
619 *FEMS Microbiol Lett* **132**: 203–208.

620 Horz, H.-P., Rich, V., Avrahami, S., and Bohannan, B.J.M. (2005) Methane-oxidizing bacteria in
621 a California upland grassland soil: diversity and response to simulated global change. *Appl*
622 *Environ Microbiol* **71**: 2642–2652.

623 Hu, B., Shen, L., Lian, X., Zhu, Q., Liu, S., Huang, Q., et al. (2014) Evidence for nitrite-
624 dependent anaerobic methane oxidation as a previously overlooked microbial methane sink
625 in wetlands. *Proc Natl Acad Sci* **111**: 4495 LP – 4500.

626 Hütsch, B.W. (1998) Tillage and land use effects on methane oxidation rates and their vertical
627 profiles in soil. *Biol Fertil Soils* **27**: 284–292.

628 Hütsch, B.W., Webster, C.P., and Powlson, D.S. (1994) Methane oxidation in soil as affected by
629 land use, soil pH and N fertilization. *Soil Biol Biochem* **26**: 1613–1622.

630 IBRA7 (2012) Interim Bioregionalisation for Australia, version 7.

631 Jenkins, M. and Adams, M.A. (2010) Vegetation type determines heterotrophic respiration in
632 subalpine Australian ecosystems. *Glob Chang Biol* **16**: 209–219.

633 Jónsson, J.Ö.G. and Davíðsdóttir, B. (2016) Classification and valuation of soil ecosystem
634 services. *Agric Syst* **145**: 24–38.

635 Kalyuzhnaya, M.G., Yang, S., Rozova, O.N., Smalley, N.E., Clubb, J., Lamb, A., et al. (2013)
636 Highly efficient methane biocatalysis revealed in a methanotrophic bacterium. *Nat Commun*
637 **4**: 2785.

638 Karbin, S., Hagedorn, F., Hiltbrunner, D., Zimmermann, S., and Niklaus, P.A. (2016) Spatial
639 micro-distribution of methanotrophic activity along a 120-year afforestation
640 chronosequence. *Plant Soil* **415**: 1–11.

641 Khadem, A.F., Wieczorek, A.S., Pol, A., Vuilleumier, S., Harhangi, H.R., Dunfield, P.F., et al.
642 (2012) Draft Genome Sequence of the Volcano-Inhabiting Thermoacidophilic
643 Methanotroph <span class="named-content genus-species" id="named-
644 content-1">Methylacidiphilum fumariolicum Strain SolV. *J*
645 *Bacteriol* **194**: 3729 LP – 3730.

646 Kirschke, S., Bousquet, P., Ciais, P., Saunois, M., Canadell, J.G., Dlugokencky, E.J., et al.
647 (2013) Three decades of global methane sources and sinks. *Nat Geosci* **6**: 813–823.

648 Kits, K.D., Campbell, D.J., Rosana, A.R., and Stein, L.Y. (2015) Diverse electron sources
649 support denitrification under hypoxia in the obligate methanotroph Methylomicrobium
650 album strain BG8 . *Front Microbiol* **6**: 1072.

651 Knief, C. (2015) Diversity and habitat preferences of cultivated and uncultivated aerobic
652 methanotrophic nacteria evaluated based on pmoA as molecular marker. *Front Microbiol* **6**:
653 1346.

654 Knief, C., Lipski, A., and Dunfield, P.F. (2003) Diversity and activity of methanotrophic bacteria
655 in different upland soils. *Appl Environ Microbiol* **69**: 6703–6714.

Kolb, S. (2009) The quest for atmospheric methane oxidizers in forest soils. *Environ Microbiol Rep* **1**: 336–346.

Kolb, S., Knief, C., Dunfield, P.F., and Conrad, R. (2005) Abundance and activity of uncultured methanotrophic bacteria involved in the consumption of atmospheric methane in two forest soils. *Environ Microbiol* **7**: 1150–1161.

Kolb, S., Knief, C., Stubner, S., and Conrad, R. (2003) Quantitative detection of methanotrophs in soil by novel pmoA-targeted Real-Time PCR assays. *Appl Environ Microbiol* **69**: 2423–2429.

Koschorreck, M. and Conrad, R. (1993) Oxidation of atmospheric methane in soil: Measurements in the field, in soil cores and in soil samples. *Global Biogeochem Cycles* **7**: 109–121.

Krause, S., Meima-Franke, M., Hefting, M.M., and Bodelier, P.L.E. (2013) Spatial patterns of methanotrophic communities along a hydrological gradient in a riparian wetland. *FEMS Microbiol Ecol* **86**: 59–70.

Luesken, F.A., Wu, M.L., Op den Camp, H.J.M., Keltjens, J.T., Stunnenberg, H., Francoijs, K., et al. (2012) Effect of oxygen on the anaerobic methanotroph 'Candidatus Methylomirabilis oxyfera': kinetic and transcriptional analysis. *Environ Microbiol* **14**: 1024–1034.

Malghani, S., Reim, A., von Fischer, J., Conrad, R., Kuebler, K., and Trumbore, S.E. (2016) Soil methanotroph abundance and community composition are not influenced by substrate availability in laboratory incubations. *Soil Biol Biochem* **101**: 184–194.

Martin, M. (2011) Cutadapt removes adapter sequences from high-throughput sequencing reads.

677 *EMBnet J* **17**: pp-10.

678 McDaniel, M.D., Kaye, J.P., and Kaye, M.W. (2014) Do “hot moments” become hotter under
679 climate change? Soil nitrogen dynamics from a climate manipulation experiment in a post-
680 harvest forest. *Biogeochemistry* **121**: 339–354.

681 McDaniel, M.D., Simpson, R.R., Malone, B.P., McBratney, A.B., Minasny, B., and Adams,
682 M.A. (2017) Quantifying and predicting spatio-temporal variability of soil CH4 and N2O
683 fluxes from a seemingly homogeneous Australian agricultural field. *Agric Ecosyst Environ*
684 **240**: 182–193.

685 Le Mer, J. and Roger, P. (2001) Production, oxidation, emission and consumption of methane by
686 soils: A review. *Eur J Soil Biol* **37**: 25–50.

687 Murrell, J.C. and Jetten, M.S.M. (2009) The microbial methane cycle. *Environ Microbiol Rep* **1**:
688 279–284.

689 Nazaries, L., Murrell, J.C., Millard, P., Baggs, L., and Singh, B.K. (2013) Methane, microbes
690 and models: fundamental understanding of the soil methane cycle for future predictions.
691 *Environ Microbiol* **15**: 2395–2417.

692 Nazaries, L., Pan, Y., Bodrossy, L., Baggs, E.M., Millard, P., Murrell, J.C., and Singh, B.K.
693 (2013) Evidence of microbial regulation of biogeochemical cycles from a study on methane
694 flux and land use change. *Appl Environ Microbiol* **79**: 4031–4040.

695 Nazaries, L., Tate, K.R., Ross, D.J., Singh, J., Dando, J., Saggar, S., et al. (2011) Response of
696 methanotrophic communities to afforestation and reforestation in New Zealand. *ISME J* **5**:
697 1832–1836.

698 Ni, X. and Groffman, P.M. (2018) Declines in methane uptake in forest soils. *Proc Natl Acad Sci*
699 **115**: 8587–8590.

700 Oksanen, J., Blanchet, F.G., Kindt, R., Legendre, P., Minchin, P.R., O'Hara, R.B., et al. (2016)
701 vegan: Community Ecology Package.

702 Oremland, R.S. and Culbertson, C.W. (1992) Evaluation of methyl fluoride and dimethyl ether
703 as inhibitors of aerobic methane oxidation. *Appl Environ Microbiol* **58**: 2983–2992.

704 Pratscher, J., Dumont, M.G., and Conrad, R. (2011) Assimilation of acetate by the putative
705 atmospheric methane oxidizers belonging to the USCα clade. *Environ Microbiol* **13**: 2692–
706 2701.

707 Pratscher, J., Vollmers, J., Wiegand, S., Dumont, M.G., and Kaster, A. (2018) Unravelling the
708 identity, metabolic potential and global biogeography of the atmospheric methane-oxidizing
709 Upland Soil Cluster α. *Environ Microbiol* **20**: 1016–1029.

710 Priemé, A. and Christensen, S. (1997) Seasonal and spatial variation of methane oxidation in a
711 Danish spruce forest. *Soil Biol Biochem* **29**: 1165–1172.

712 Priemé, A., Christensen, S., Dobbie, K.E., and Smith, K.A. (1997) Slow increase in rate of
713 methane oxidation in soils with time following land use change from arable agriculture to
714 woodland. *Soil Biol Biochem* **29**: 1269–1273.

715 R Core Team (2018) R: A language and environment for statistical computing.

716 Reeburgh, W.S. (2003) Global methane biogeochemistry. *Treatise on geochemistry* **4**: 347.

717 Reim, A., Hernández, M., Klose, M., Chidthaisong, A., Yuttitham, M., and Conrad, R. (2017)
718 Response of methanogenic microbial communities to desiccation stress in flooded and rain-

719 fed paddy soil from Thailand. *Front Microbiol* **8**: 785.

720 Saari, A., Martikainen, P.J., Ferm, A., Ruuskanen, J., De Boer, W., Troelstra, S.R., and
721 Laanbroek, H.J. (1997) Methane oxidation in soil profiles of Dutch and Finnish coniferous
722 forests with different soil texture and atmospheric nitrogen deposition. *Soil Biol Biochem*
723 **29**: 1625–1632.

724 Sass, R., Denmead, O.T., Conrad, R., Freney, J., Klug, M., Minami, K., et al. (1992) Exchange
725 of methane and other trace gases in rice cultivation. *Ecol Bull* 199–206.

726 Saunois, M., Bousquet, P., Poulter, B., Peregon, A., Ciais, P., Canadell, J.G., et al. (2016) The
727 global methane budget 2000–2012. *Earth Syst Sci Data* **8**: 697–751.

728 Schloss, P.D., Westcott, S.L., Ryabin, T., Hall, J.R., Hartmann, M., Hollister, E.B., et al. (2009)
729 Introducing mothur: open-source, platform-independent, community-supported software for
730 describing and comparing microbial communities. *Appl Environ Microbiol* **75**: 7537–7541.

731 Schnell, S. and King, G.M. (1994) Mechanistic analysis of ammonium inhibition of atmospheric
732 methane consumption in forest soils. *Appl Environ Microbiol* **60**: 3514–3521.

733 Sexstone, A.J., Revsbech, N.P., Parkin, T.B., and Tiedje, J.M. (1985) Direct measurement of
734 oxygen profiles and denitrification rates in soil aggregates. *Soil Sci Soc Am J* **49**: 645–651.

735 Shrestha, P.M., Kammann, C., Lenhart, K., Dam, B., and Liesack, W. (2012) Linking activity,
736 composition and seasonal dynamics of atmospheric methane oxidizers in a meadow soil.
737 *ISME J* **6**: 1115–1126.

738 Shukla, P.N., Pandey, K.D., and Mishra, V.K. (2013) Environmental determinants of soil
739 methane oxidation and methanotrophs. *Crit Rev Environ Sci Technol* **43**: 1945–2011.

740 SILO - Queensland Government.

741 Singh, J.S., Singh, Smita, Raghubanshi, A.S., Singh, Saranath, Kashyap, A.K., and Reddy, V.S.
742 (1997) Effect of soil nitrogen, carbon and moisture on methane uptake by dry tropical forest
743 soils. *Plant Soil* **196**: 115–121.

744 Singleton, C.M., McCalley, C.K., Woodcroft, B.J., Boyd, J.A., Evans, P.N., Hodgkins, S.B., et
745 al. (2018) Methanotrophy across a natural permafrost thaw environment. *ISME J* **12**: 2544–
746 2558.

747 Smith, K.A., Dobbie, K.E., Ball, B.C., Bakken, L.R., Sitaula, B.K., Hansen, S., et al. (2000)
748 Oxidation of atmospheric methane in Northern European soils, comparison with other
749 ecosystems, and uncertainties in the global terrestrial sink. *Glob Chang Biol* **6**: 791–803.

750 Stocker, D.Q. (2013) Climate change 2013: The physical science basis. *Work Gr I Contrib to*
751 *Fifth Assess Rep Intergov Panel Clim Chang Summ Policymakers, IPCC*.

752 Sullivan, B.W., Kolb, T.E., Hart, S.C., Kaye, J.P., Hungate, B.A., Dore, S., and Montes-Helu, M.
753 (2010) Wildfire reduces carbon dioxide efflux and increases methane uptake in ponderosa
754 pine forest soils of the southwestern USA. *Biogeochemistry* **104**: 251–265.

755 Sullivan, B.W., Selmants, P.C., and Hart, S.C. (2013) Does dissolved organic carbon regulate
756 biological methane oxidation in semiarid soils? *Glob Chang Biol* **19**: 2149–2157.

757 Tarboton, D.G. (2005) Terrain analysis using digital elevation models (TauDEM). *Utah State*
758 *Univ Logan*.

759 Thauer, R.K., Kaster, A.-K., Seedorf, H., Buckel, W., and Hedderich, R. (2008) Methanogenic
760 archaea: ecologically relevant differences in energy conservation. *Nat Rev Microbiol* **6**:

579–591.

Tilman, D., Reich, P.B., Knops, J., Wedin, D., Mielke, T., and Lehman, C. (2001) Diversity and productivity in a long-term grassland experiment. *Science (80-)* **294**: 843–845.

Tveit, A.T., Hestnes, A.G., Robinson, S.L., Schintlmeister, A., Dedysh, S.N., Jehmlich, N., et al. (2019) Widespread soil bacterium that oxidizes atmospheric methane. *Proc Natl Acad Sci* **116**: 8515 LP – 8524.

Velthof, G.L., Jarvis, S.C., Stein, A., Allen, A.G., and Oenema, O. (1996) Spatial variability of nitrous oxide fluxes in mown and grazed grasslands on a poorly drained clay soil. *Soil Biol Biochem* **28**: 1215–1225.

Warnes, G., Bolker, B., and Lumley, T. (2015) gplots: various R programming tools for plotting data. R package version 2.6.0.

Wille, C., Kutzbach, L., Sachs, T., Wagner, D., and Pfeiffer, E.M. (2008) Methane emission from Siberian arctic polygonal tundra: Eddy covariance measurements and modeling. *Glob Chang Biol* **14**: 1395–1408.

Wolf, K., Flessa, H., and Veldkamp, E. (2012) Atmospheric methane uptake by tropical montane forest soils and the contribution of organic layers. *Biogeochemistry* **111**: 469–483.

Wu, X., Yao, Z., Brüggemann, N., Shen, Z.Y., Wolf, B., Dannenmann, M., et al. (2010) Effects of soil moisture and temperature on CO2 and CH4 soil–atmosphere exchange of various land use/cover types in a semi-arid grassland in Inner Mongolia, China. *Soil Biol Biochem* **42**: 773–787.

Yabe, S., Sakai, Y., Abe, K., and Yokota, A. (2017) Diversity of Ktedonobacteria with

Actinomycetes-Like Morphology in Terrestrial Environments. *Microbes Environ* **32**: 61–70.

Yang, W.H. and Silver, W.L. (2016) Net soil-atmosphere fluxes mask patterns in gross production and consumption of nitrous oxide and methane in a managed ecosystem. *Biogeosciences* **13**: 1705.

Yokota, A. (2012) Cultivation of uncultured bacteria of the class Ktedonobacteria in the Phylum Chloroflexi. *Makara J Sci* **1**: 1–8.

Yu, Y., Lee, C., Kim, J., and Hwang, S. (2005) Group-specific primer and probe sets to detect methanogenic communities using quantitative real-time polymerase chain reaction. *Biotechnol Bioeng* **89**: 670–679.

Zhou, J., Xia, B., Treves, D.S., Wu, L.-Y., Marsh, T.L., O'Neill, R. V, et al. (2002) Spatial and resource factors influencing high microbial diversity in soil. *Appl Environ Microbiol* **68**: 326–334.

Zuur, A.F., Ieno, E.N., and Elphick, C.S. (2010) A protocol for data exploration to avoid common statistical problems. *Methods Ecol Evol* **1**: 3–14.

Table 1. Annual estimates (mean, standard error, and range) for net ecosystem flux of carbon dioxide and methane

Ecosystem	% of 548 ha Watershed*	Net Ecosystem Flux	
		CO_2	CH_4
		CO_2-equivalents g m^{-2} y^{-1}	
Forest	8-75	911 ± 165	-506 ± 22
Grassland	25-91	484 ± 50	-259 ± 38
Bog	1	646 ± 109	256 ± 82
		CO_2-equivalents kg ha^{-1} y^{-1}	
Total Watershed		5207 to 8031	-2762 to -4391

Table 2. Comparison of Global and Australian Alps soil methane sink estimates

Measurement	Values		
Ecosystems Areal Coverage			
Global forest+grassland ecosystems (millions of ha)	5,100		
Areal coverage of Australian Alps – Figure 8 (millions of ha)	1.23		
Fraction of Australian Alps to global forest+grassland (%)	0.024		
Soil CH_4 Sink Estimates	**Low Estimate**	**Best Estimate**	**High Estimate**
Global CH_4 Soil Sink† *(Tg y^{-1})*	-9	-30	-100
Mean annual Australian Alps CH_4 sink‡ (kg ha^{-1} y^{-1})	-4.2	-19.2	-33.2
Australian Alps Contribution to Global CH_4 Sink (%)	**Low Estimate**	**Best Estimate**	**High Estimate**
Low estimate (-6.2 kg ha^{-1} y^{-1})	69	21	6
Best Estimate, or our projection (-19.2 kg ha^{-1} y^{-1})	213	64	19
High estimate (-32.3 kg ha^{-1} y^{-1})	359	108	32

†: Low and Best Estimates from Kirschke et al. (2013) and Saunois et al. (2016). Other estimates have a high estimates of -100 Tg y^{-1} (Smith et al. 2000)

‡: Based on forest foliage imagery, soil temperatures and moisture estimates, and CH_4 modeling described in Experimental Procedures. High and Low estimate from +/- relative standard deviation from ecosystem means.

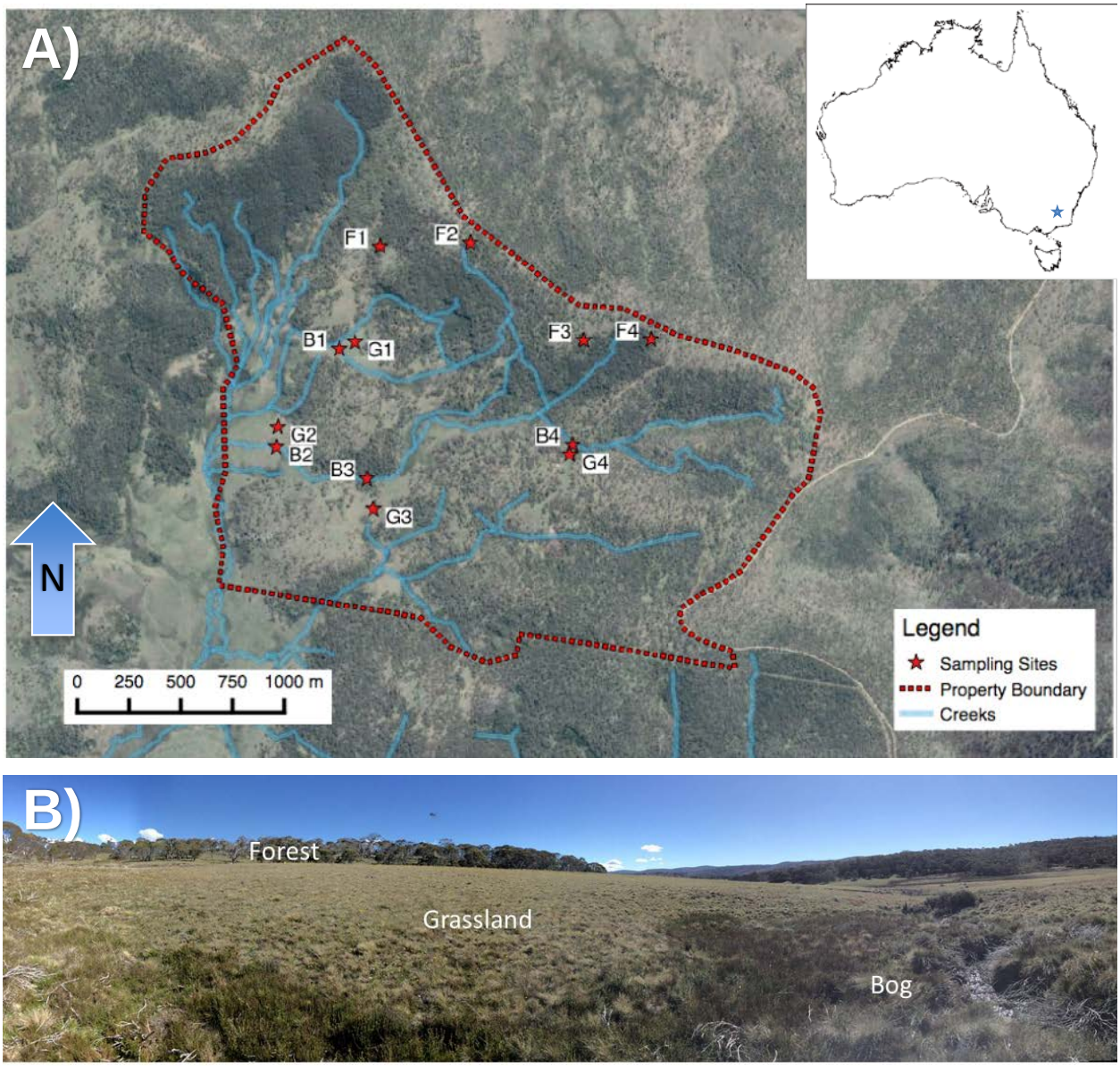

Fig. 1. **A)** Location of 548 ha experiment area (inset of Australia), sampling sites within area and nearby streams. **B)** Landscape-level photograph of the vegetation gradient from sphagnum-dominated bog in foreground to eucalyptus-dominated forest in background. Abbreviations are F = Forest, G = Grassland, and B = Bog. The numbers after the letter represent which transect the sampling location belongs to.

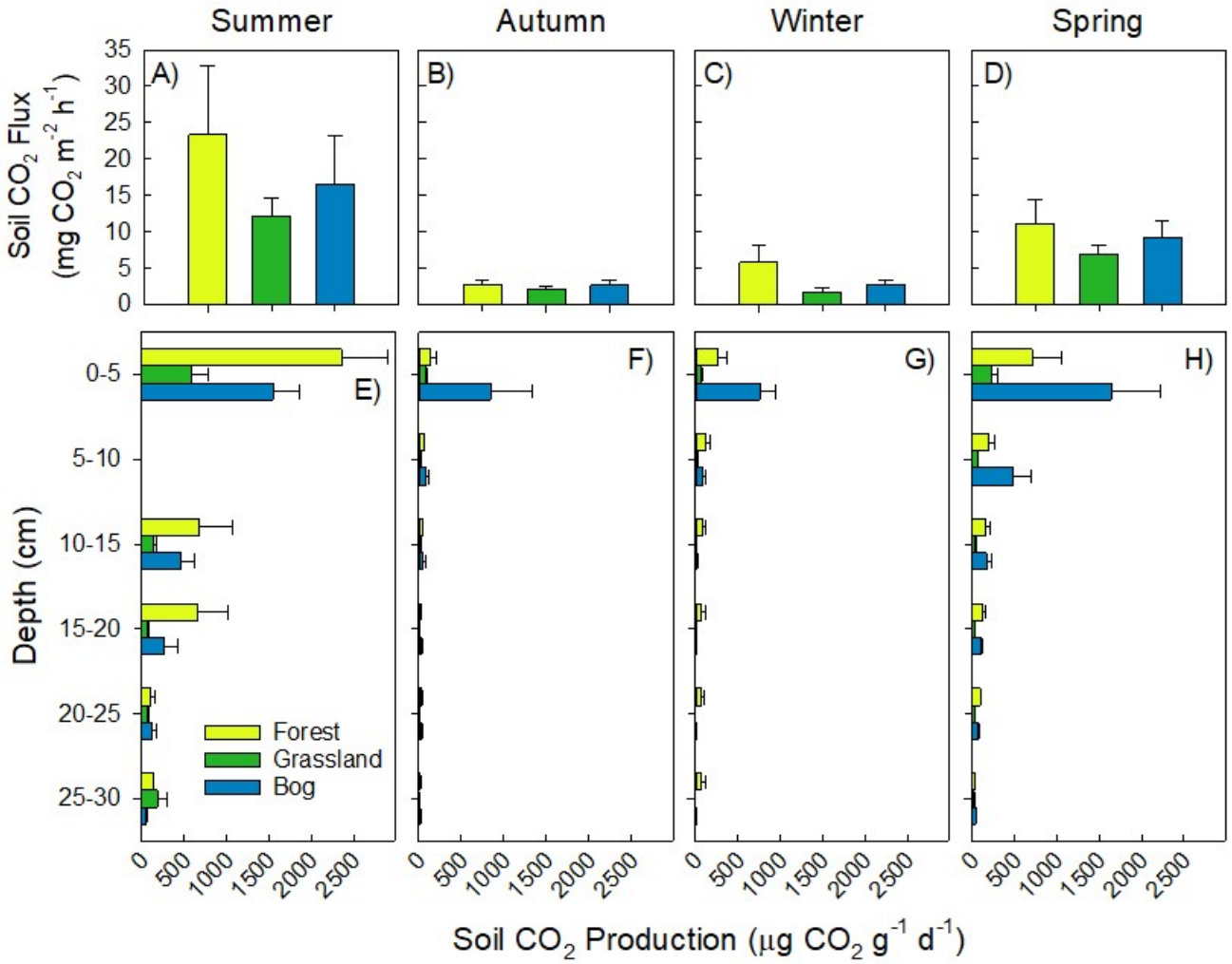

Fig. 2. Soil CO_2 fluxes (top panels, **A-D**) and production (bottom panels, **E-H**). Surface flux measurements and soils collected for production on 17 February (Summer,**A** & **E**), 25 May (Autumn, **B** & **F**), 22 September (Winter, **C** & **G**), and 23 November (Spring, **D** & **H**) in 2015. Mean and standard error shown (n = 4).

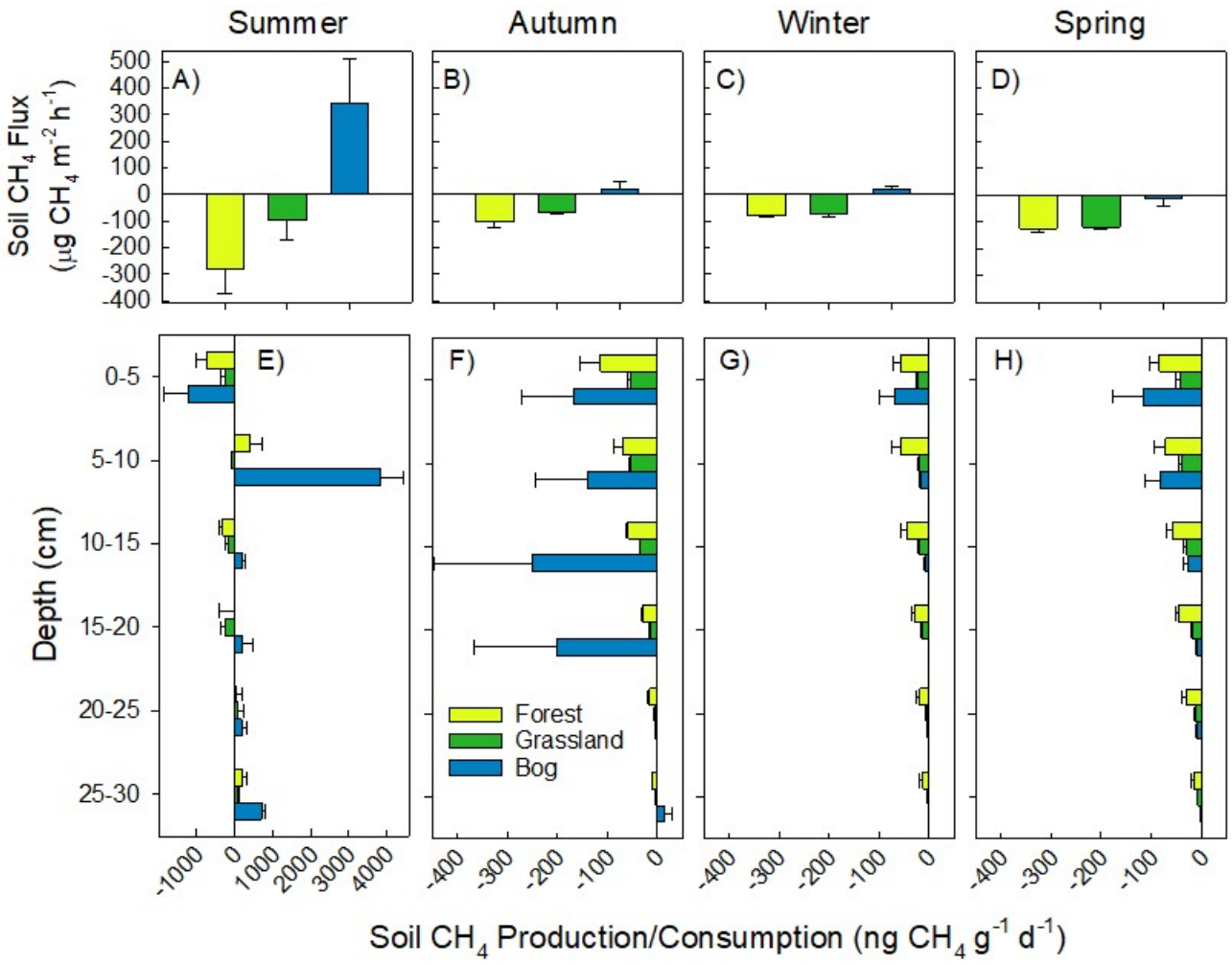

Fig. 3. Soil CH_4 fluxes (top panels, **A-D**) and production/consumption (bottom panels, **E-H**). Surface flux measurements and soils collected for production on 17 February (Summer,A & E), 25 May (Autumn, **B** & F), 22 September (Winter, **C** & **G**), and 23 November (Spring, **D** & **H**) in 2015. Mean and standard error shown (n = 4).

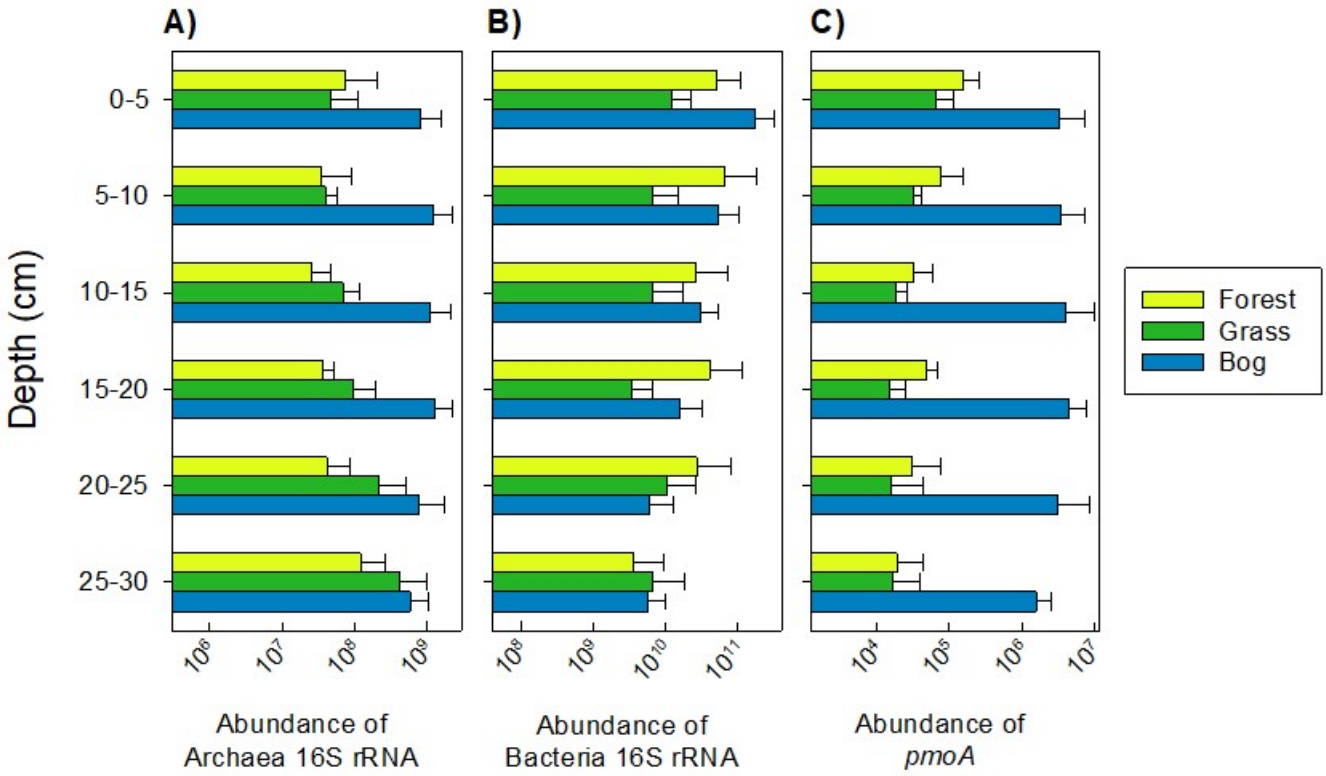

Fig. 4. Abundance of archaeal (**A**) and bacterial (**B**) 16S rRNA genes, and *pmoA* (C). Means and standard error are shown (n=4) for all samples.

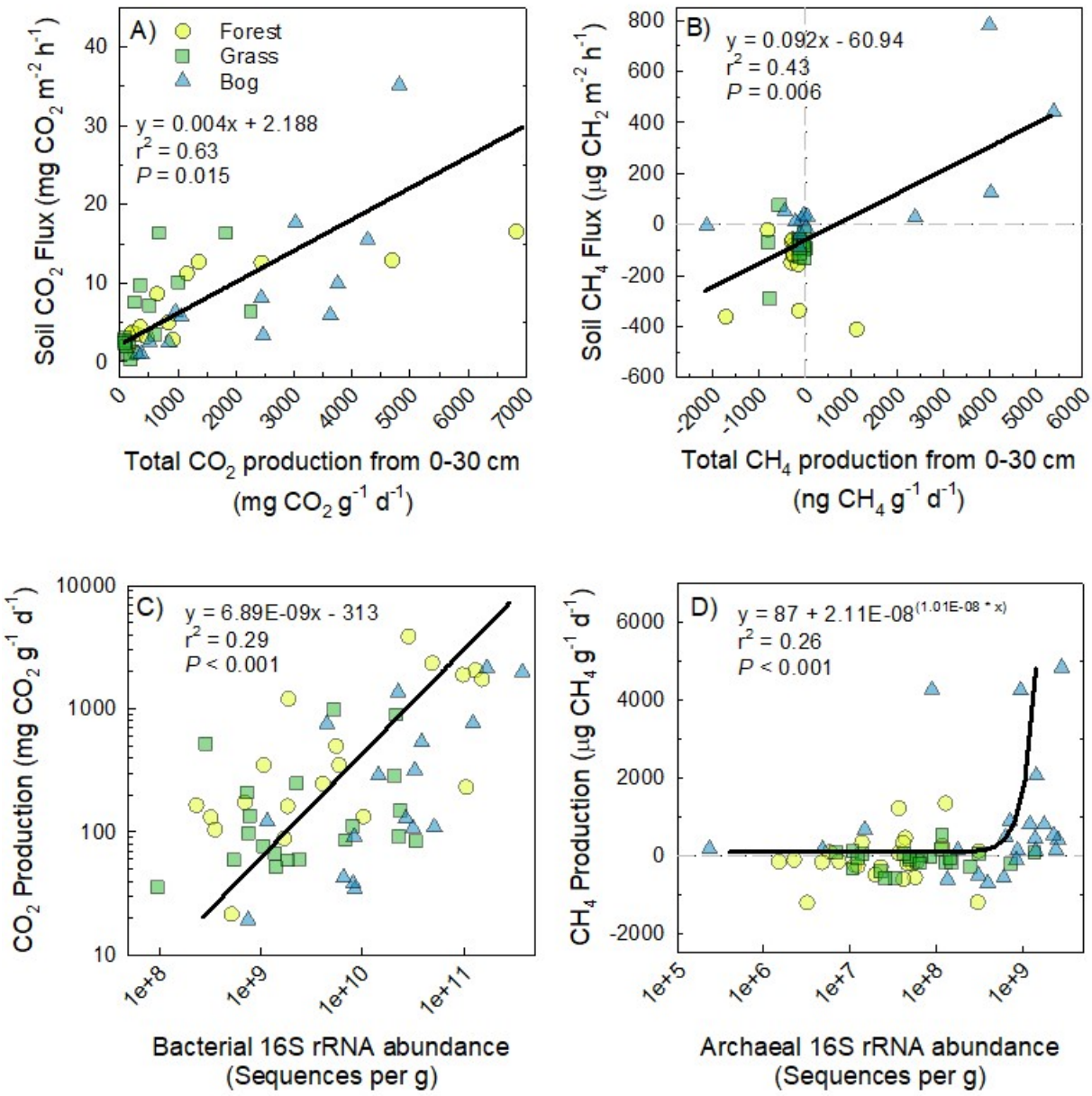

Fig. 5. Regressions between total CO_2 production and CO_2 soil-atmosphere flux (**A**), CH_4 production and CH_4 soil-atmosphere flux (**B**). Total GHG production was calculated for each soil profile as sum of production from 0 to 30 cm depth. Regressions between bacterial 16S rRNA abundance with CO_2 production (**C**, linear equation with log, log scale). Regression between and archaeal 16S rRNA and CH_4 production (**D**, 3-parameter exponential, log x-axis). Equations, chosen by best fit, are shown in each panel.

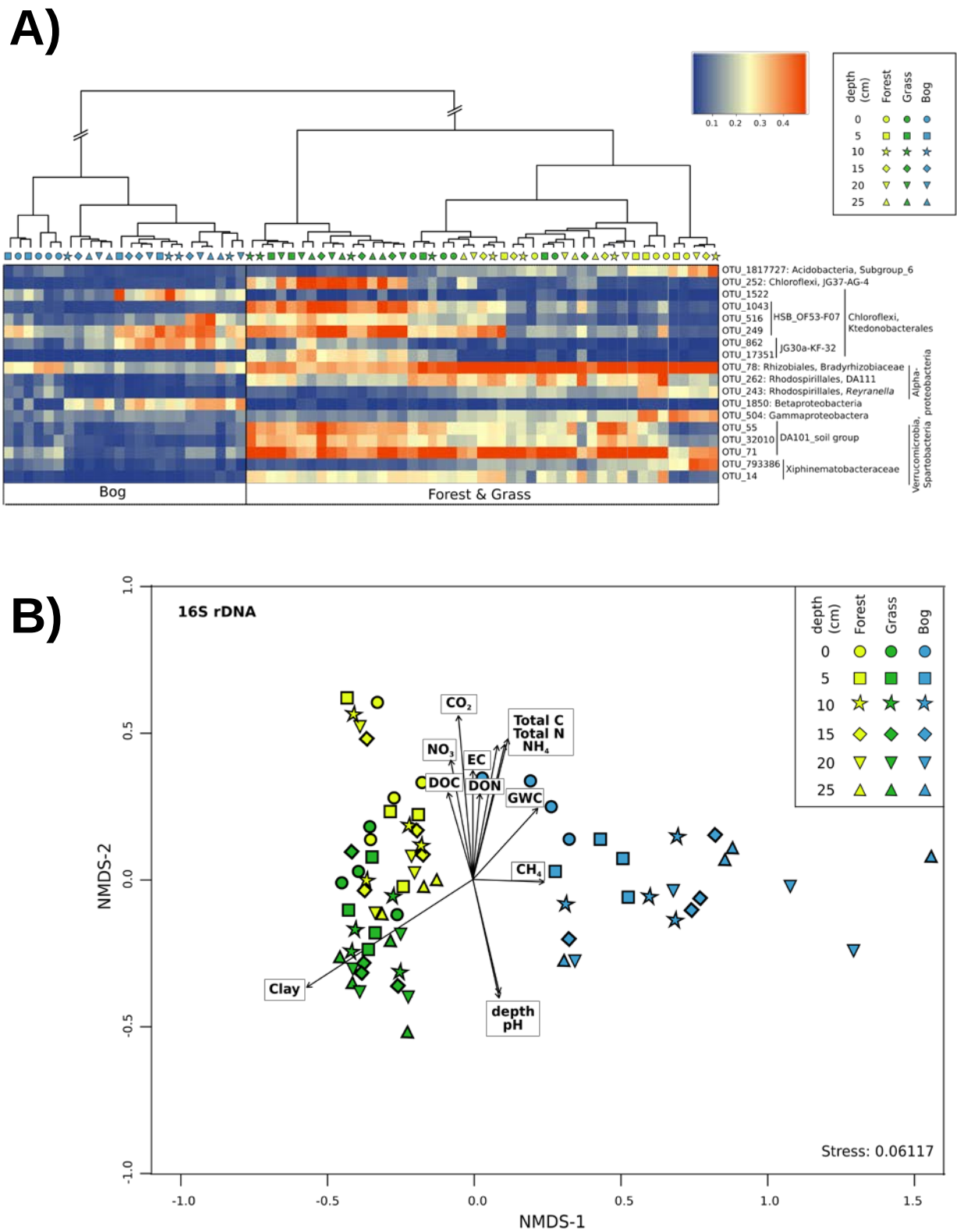

Fig. 6. **A)** Heatmap of the most relevant OTUs derived from bacterial 16S rRNA genes. The samples and OTUs were clustered according to Euclidean distances between all Hellinger transformed data. The taxonomy of OTUs was determined using the Sina classifier. The colored scale gives the percentage abundance of OTUs. **B)** NMDS ordination of bacterial 16S rRNA communities based on the Bray–Curtis dissimilarity of community composition (stress =0.061). Arrows indicate the direction at which the environmental vectors fit the best (using the *envfit* function) onto the NMDS ordination space. EC, electrical conductivity; DOC, dissolved organic carbon; DON, dissolved organic nitrogen; GWC, gravimetric water content.

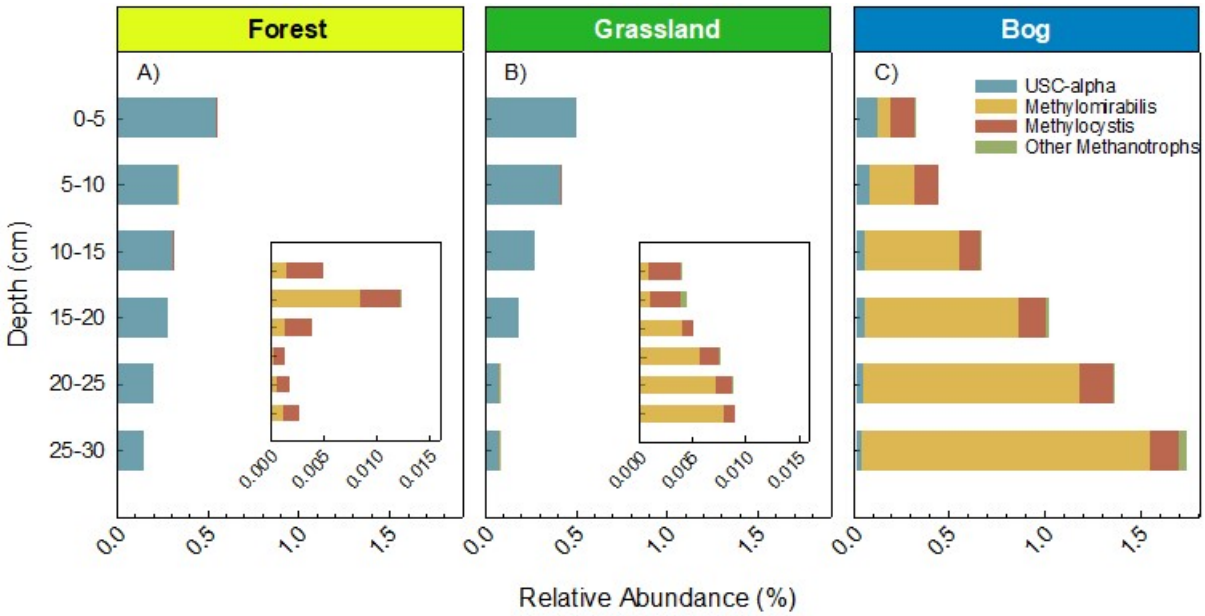

Fig. 7. Relative abundance of 16S rRNA genes of the dominant methanotroph groups detected in the forest (**A**), grass (**B**), and bog (**C**) sites. USCα was identified by blast as described in the methods. *Methylocystis* and *Methylomirabilis* were identified based on the Silva classifications. Other methanotrophs include *Methylomonas* and *Methylospira*.

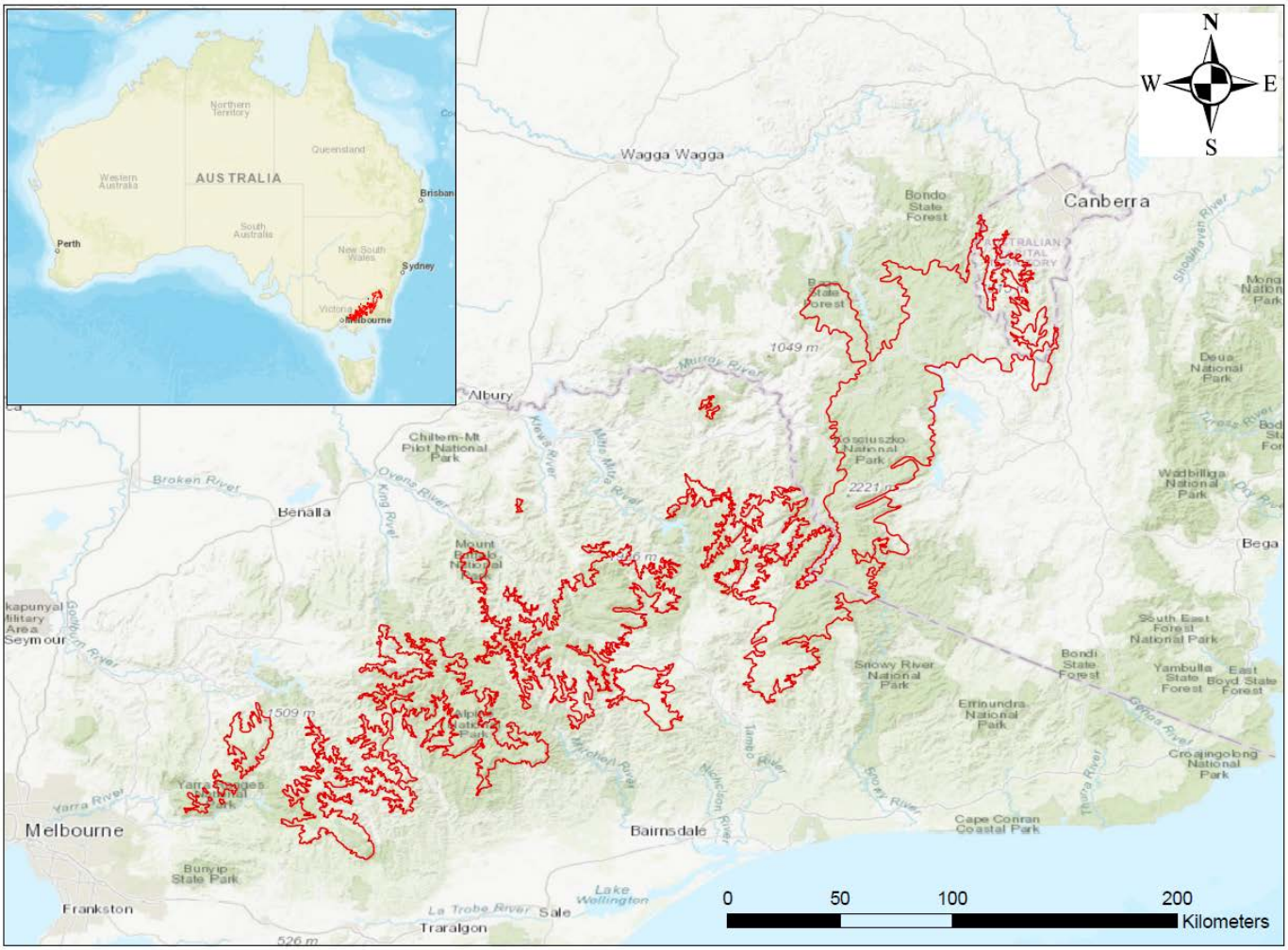

Fig. 8. Areal coverage of Australian Alps in southeastern Australia (1.2M ha).

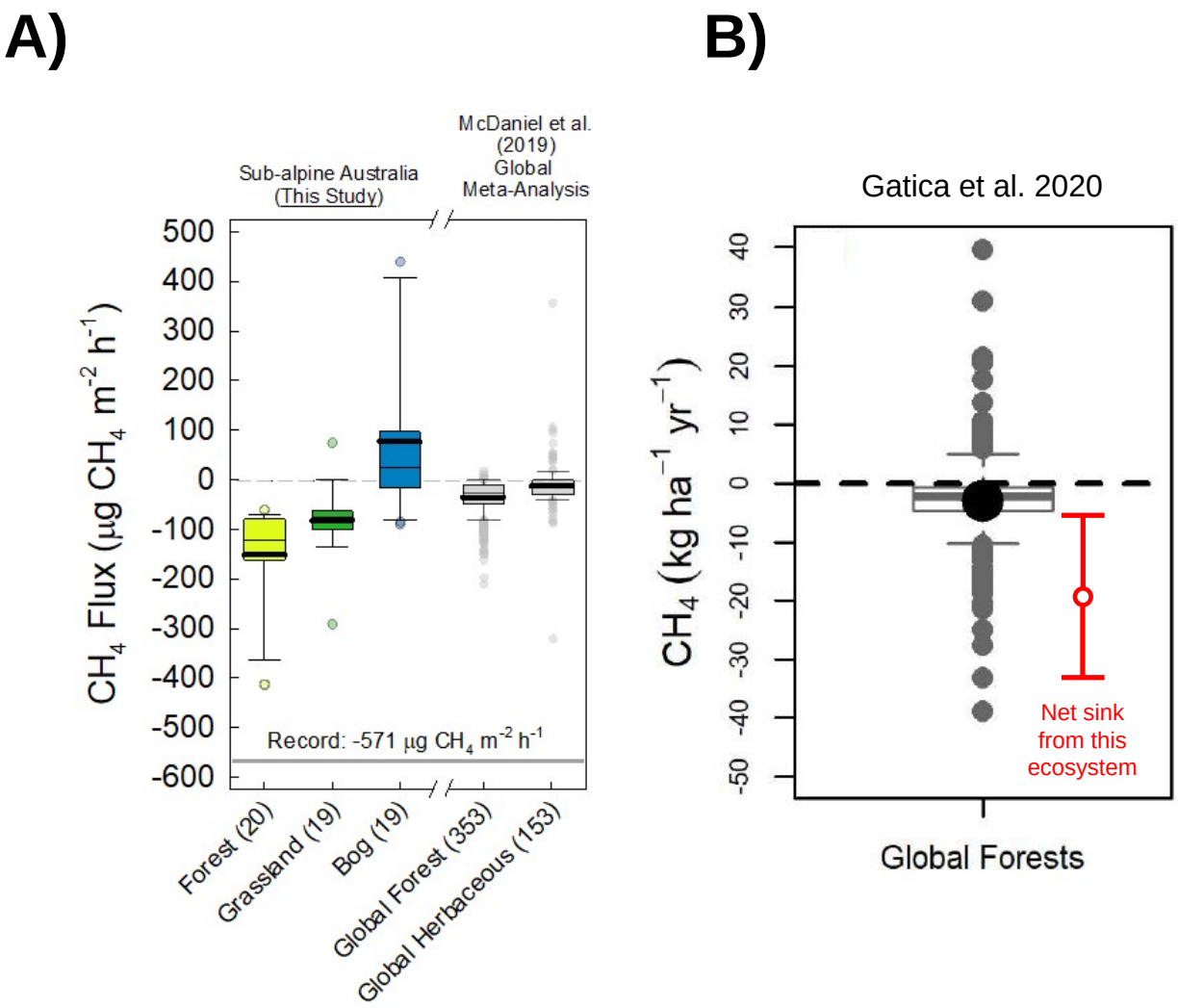

Fig. 9. **A)** Hourly methane (CH_4) fluxes from this study's Forest, Grassland and Bog soils compared to Forest and Herbaceous studies from a global meta-analysis (McDaniel et al. 2019). 10^{th} and 90^{th} percentile shown by bottom and top whisker. 25^{th} and 75^{th} percentile shown by bottom and top of the box. Median is shown by the thin line, mean by the thick line, and outliers are circles. The number of measurements within each boxplot are shown in parentheses. Gray bar at -571 µg CH_4 m^{-2} h^{-1} is the greatest CH_4 oxidation rate (most negative flux) ever observed and published (Singh et al., 1997). **B)** Figure from survey of global forest CH_4 fluxes (Gatica et al. 2020) with our modeled annual mean net CH_4 sink from Australian Alps and range created ± relative standard deviation from ecosystem means (Table 2).

Supplementary Information

Disproportionate CH_4 sink strength from an endemic, sub-alpine Australian soil microbial community

M.D. McDaniel1,2*‡, M. Hernández3,4*, M.G. Dumont3,5, L.J. Ingram1, and M.A. Adams1,6

1. Centre for Carbon Water and Food | Sydney Institute of Agriculture | University of Sydney | Sydney, Australia 2000
2. Department of Agronomy | Iowa State University | Ames, Iowa USA 50011
3. Max Planck Institute for Terrestrial Microbiology | Marburg, Germany D-35037
4. School of Environmental Sciences | Norwich Research Park | University of East Anglia, Norwich, UK NR4 7TJ
5. Centre for Biological Sciences | University of Southampton | Southampton, UK SO17 1BJ
6. School of Science | Engineering and Technology | The University of Swinburne | Melbourne, Australia 3122

Supplementary Information Table of Contents

TABLES

FIGURES

Table S1. Chamber and soil microclimate at time of sampling, and incubation temperature by date in 2015 (means ± standard errors)†

Date	Soil-Vegetation Type	GHG Chamber Temperature	Soil Temperature	Incubation Room Temperature Range‡	Volumetric Moisture Content
		---------- ° C ----------			--- m^3 m^{-3} ---
February 17th †	Forest	20.5 ± 1.9	13.4 ± 0.2	20.9 to 22.5	26.7 ± 4.9
	Grassland	28.3 ± 2.1	16.4 ± 0.8		22.2 ± 1.8
	Bog	27.2 ± 3.2	14.1 ± 0.6		68.3 ± 5.7
May 25th	Forest	10.1 ± 0.9	3.9 ± 0.4	4.9 to 5.6	18.4 ± 2.3
	Grassland	7.5 ± 2.3	3.6 ± 0.2		27.2 ± 0.6
	Bog	7.5 ± 1.4	3.6 ± 0.8		77.2 ± 9.1
September 22nd	Forest	4.1 ± 0.7	4.3 ± 0.4	5.0 to 5.7	28.3 ± 3
	Grassland	5.1 ± 1	4 ± 0.3		27.1 ± 1.7
	Bog	3.1 ± 2.4	4.6 ± 0.3		85.7 ± 9.3
November 23rd	Forest	21 ± 1.7	12.7 ± 1.1	13.8 to 15.6	10.5 ± 2.2
	Grassland	17.8 ± 1.8	13 ± 1.1		14.1 ± 1.6
	Bog	16.3 ± 1.9	11.5 ± 0.8		57.5 ± 9.6

†: Date of soil microbial community analyses.

‡: Intended to correspond to field conditions as close as possible

Table S2. Dynamic soil physical and chemical characteristics by date in 2015 (means ± standard errors)[†]

Date	Soil Type	Depth (cm)	Gravimetric Water Content	Ammonium	Nitrate
			---- g g^{-1} ----	---------- mg kg^{-1} ----------	
February 17th [‡]	Forest	0 – 5	0.79 ± 0.1	73.08 ± 17.87	7.57 ± 7.27
		5 – 10	0.57 ± 0.2	63.92 ± 31.45	3.66 ± 3.41
		10 – 15	0.52 ± 0.18	49.26 ± 22.93	1.55 ± 1.37
		15 – 20	0.43 ± 0.13	39.62 ± 15.13	1.15 ± 0.8
		20 – 25	0.43 ± 0.14	35.12 ± 17.22	0.71 ± 0.47
		25 – 30	0.25 ± 0.02	16.94 ± 1.81	0.41 ± 0.16
	Grassland	0 – 5	0.38 ± 0.06	37.69 ± 4.54	0.75 ± 0.29
		5 – 10	0.34 ± 0.03	26.08 ± 1.81	0.47 ± 0.1
		10 – 15	0.31 ± 0.03	19.49 ± 1.73	0.54 ± 0.13
		15 – 20	0.28 ± 0.03	15.09 ± 1	0.43 ± 0.06
		20 – 25	0.29 ± 0.05	13.41 ± 0.85	0.45 ± 0.07
		25 – 30	0.25 ± 0.03	11.21 ± 0.48	0.58 ± 0.04
	Bog	0 – 5	4.66 ± 0.92	205.81 ± 21.75	0.61 ± 0.1
		5 – 10	5.83 ± 3.45	160.3 ± 34.53	0.29 ± 0.06
		10 – 15	2.29 ± 0.9	82.27 ± 23.49	0.21 ± 0.01
		15 – 20	1.16 ± 0.23	38.18 ± 11.53	0.27 ± 0.05
		20 – 25	1.36 ± 0.43	32.06 ± 11.11	0.2 ± 0.03
		25 – 30	0.93 ± 0.15	19.35 ± 5.92	0.16 ± 0.03
May 25th	Forest	0 – 5	0.8 ± 0.19	3.17 ± 0.8	0.21 ± 0.08
		5 – 10	0.46 ± 0.07	3.47 ± 0.43	0.18 ± 0.11
		10 – 15	0.46 ± 0.1	4.31 ± 1.18	0.25 ± 0.1
		15 – 20	0.42 ± 0.09	3.53 ± 0.26	0.16 ± 0.07
		20 – 25	0.42 ± 0.1	2.83 ± 0.38	0.17 ± 0.06
		25 – 30	0.32 ± 0.05	2.86 ± 0.31	0.22 ± 0.12
	Grassland	0 – 5	0.43 ± 0.04	60.31 ± 3.72	BDL
		5 – 10	0.37 ± 0.02	40.78 ± 0.45	1.28 ± 0.83
		10 – 15	0.35 ± 0.02	30.68 ± 1.63	0.71 ± 0.15
		15 – 20	0.34 ± 0.02	23.75 ± 0.83	0.15 ± 0.04
		20 – 25	0.32 ± 0.02	19.47 ± 1.18	BDL
		25 – 30	0.31 ± 0.02	17.7 ± 2.06	0.29 ± 0.12
	Bog	0 – 5	8.7 ± 5.21	109.63 ± 46.63	0.49 ± 0.03
		5 – 10	3.58 ± 1.78	70.63 ± 35.02	0.87 ± 0.28
		10 – 15	4.75 ± 2.77	98.8 ± 16.42	0.42 ± 0.14
		15 – 20	12.5 ± 9.84	36.69 ± 0	0.94 ± 0.01
		20 – 25	1.55 ± 0.33	36.65 ± 2.59	BDL
		25 – 30	1.06 ± 0.27	7.29 ± 4.57	0.24 ± 0.1
September 22nd	Forest	0 – 5	0.91 ± 0.25	126.08 ± 10.56	2.14 ± 1.55
		5 – 10	0.56 ± 0.14	67.03 ± 10.03	1.46 ± 1
		10 – 15	0.52 ± 0.13	54.36 ± 9.17	0.9 ± 0.56
		15 – 20	0.47 ± 0.09	58.92 ± 14.93	0.8 ± 0.5
		20 – 25	0.44 ± 0.08	51.63 ± 14.74	0.48 ± 0.22
		25 – 30	0.42 ± 0.11	35.61 ± 10.14	0.4 ± 0.09
	Grassland	0 – 5	0.45 ± 0.03	94.52 ± 7.72	0.71 ± 0.24
		5 – 10	0.36 ± 0.02	87.32 ± 24.64	0.83 ± 0.14
		10 – 15	0.34 ± 0.02	37.95 ± 5.23	0.85 ± 0.24
		15 – 20	0.32 ± 0.02	26.73 ± 3.46	1.01 ± 0.12
		20 – 25	0.3 ± 0.02	19.89 ± 2.6	0.86 ± 0.14
		25 – 30	0.29 ± 0.02	17.9 ± 1.23	1.03 ± 0.11
	Bog	0 – 5	4.93 ± 1.34	152.3 ± 6.16	0.26 ± 0.03
		5 – 10	1.91 ± 0.25	128.86 ± 30.83	0.28 ± 0.03
		10 – 15	1.12 ± 0.22	73.28 ± 28.6	0.19 ± 0.01
		15 – 20	1.24 ± 0.23	85.1 ± 29.85	0.23 ± 0
		20 – 25	1.3 ± 0.06	78 ± 12.68	0.18 ± 0.03

		25 – 30	0.94 ± 0.03	42.34 ± 4.62	BDL
November 23rd	Forest	0 – 5	0.55 ± 0.06	140.41 ± 16.54	BDL
		5 – 10	0.4 ± 0.06	76.66 ± 13.65	BDL
		10 – 15	0.34 ± 0.06	61.67 ± 9.83	BDL
		15 – 20	0.3 ± 0.04	47.32 ± 7.09	BDL
		20 – 25	0.26 ± 0.03	36.05 ± 1.91	BDL
		25 – 30	0.25 ± 0.01	21.73 ± 0.37	BDL
	Grassland	0 – 5	0.26 ± 0.04	76.44 ± 7.66	BDL
		5 – 10	0.29 ± 0.02	64.11 ± 6.2	BDL
		10 – 15	0.29 ± 0.02	47.18 ± 4.03	BDL
		15 – 20	0.29 ± 0.02	35.76 ± 3.38	BDL
		20 – 25	0.28 ± 0.03	32.34 ± 2.45	BDL
		25 – 30	0.27 ± 0.03	26.16 ± 1.6	BDL
	Bog	0 – 5	3.87 ± 1.53	224.65 ± 6.23	0.41 ± 0.13
		5 – 10	3.19 ± 1.28	223 ± 42.37	BDL
		10 – 15	2.35 ± 0.81	191.28 ± 52.98	BDL
		15 – 20	1.6 ± 0.61	90.36 ± 27.71	BDL
		20 – 25	0.95 ± 0.25	30.89 ± 8.46	BDL
		25 – 30	0.68 ± 0.15	ND	ND

†: BDL, soil extract below detection limit (0.03 mg L^{-1}); ND, no data

‡: Date of soil microbial community analyses.

Table S3. Static soil physical and chemical characteristics – from 17 February 2015 (means ± standard errors)

Soil Type	Depth (cm)	Sand	Silt	Clay	Gravel & Rocks	Roots or Rhizoids	pH	Total Organic Carbon	Total Nitrogen
		---------- % ----------			---------- g cm^{-3} ---------			---------- % ----------	
Forest	0 – 5	74 ± 0	9 ± 1	17 ± 1	64 ± 20	9.68 ± 1.24	5.46 ± 0.14	10.11 ± 1.30	0.58 ± 0.08
	5 – 10	73 ± 1	12 ± 1	15 ± 1	88 ± 33	2.05 ± 0.69	5.45 ± 0.22	7.90 ± 1.93	0.44 ± 0.12
	10 – 15	72 ± 3	13 ± 2	14 ± 1	114 ± 34	3.06 ± 1.18	5.50 ± 0.14	5.46 ± 0.97	0.31 ± 0.07
	15 – 20	76 ± 2	9 ± 1	15 ± 1	90 ± 16	1.42 ± 0.73	5.51 ± 0.15	4.88 ± 1.12	0.27 ± 0.08
	20 – 25	72 ± 2	13 ± 3	14 ± 2	100 ± 19	3.67 ± 1.01	5.53 ± 0.10	4.63 ± 1.11	0.25 ± 0.07
	25 – 30	68 ± 2	16 ± 2	16 ± 2	134 ± 26	1.30 ± 0.86	5.55 ± 0.09	4.11 ± 1.06	0.22 ± 0.06
Grassland	0 – 5	64 ± 3	15 ± 2	22 ± 2	17 ± 4	5.35 ± 1.27	5.54 ± 0.08	5.97 ± 0.42	0.41 ± 0.03
	5 – 10	55 ± 3	20 ± 1	24 ± 3	20 ± 5	0.28 ± 0.13	5.54 ± 0.06	4.67 ± 0.19	0.32 ± 0.01
	10 – 15	56 ± 2	20 ± 2	24 ± 2	11 ± 3	0.22 ± 0.12	5.49 ± 0.05	3.86 ± 0.11	0.26 ± 0.01
	15 – 20	53 ± 2	21 ± 3	26 ± 2	13 ± 3	0.09 ± 0.03	5.52 ± 0.04	3.1 ± 0.19	0.21 ± 0.01
	20 – 25	54 ± 3	20 ± 3	25 ± 2	17 ± 4	1.21 ± 1.12	5.52 ± 0.06	2.61 ± 0.17	0.18 ± 0.01
	25 – 30	55 ± 3	20 ± 3	24 ± 1	22 ± 3	0.05 ± 0.04	5.58 ± 0.08	2.34 ± 0.22	0.16 ± 0.01
Bog	0 – 5	60 ± 6	23 ± 6	17 ± 0	7 ± 3	12.41 ± 2.03	5.38 ± 0.10	12.78 ± 0.96	0.69 ± 0.07
	5 – 10	75 ± 2	19 ± 2	6 ± 1	121 ± 67	3.79 ± 1.16	5.51 ± 0.04	9.59 ± 4.26	0.54 ± 0.18
	10 – 15	80 ± 2	14 ± 3	6 ± 1	72 ± 44	1.01 ± 0.19	5.58 ± 0.02	11.47 ± 3.27	0.72 ± 0.14
	15 – 20	79 ± 3	15 ± 2	6 ± 1	119 ± 57	1.30 ± 0.26	5.53 ± 0.00	8.29 ± 2.67	0.5 ± 0.15
	20 – 25	82 ± 1	11 ± 2	7 ± 0	203 ± 63	2.52 ± 1.07	5.63 ± 0.02	5.82 ± 0.76	0.34 ± 0.07
	25 – 30	82 ± 5	11 ± 3	7 ± 2	129 ± 46	2.05 ± 0.58	5.69 ± 0.02	3.72 ± 0.72	0.2 ± 0.04

Table S4. Barcode identification for each of the samples analyzed. Raw data were deposited under the study accession number PRJNA384296 in the NCBI Sequence Read Archive (SRA). For 16S rRNA genes, primers used: F515 (5'-GTGCCAGCMGCCGCGGTAA-3'), R806 (5'-GGACTACVSGGGTATCTAAT-3'). For *pmoA* genes, primer set first round PCR (A189f/A682r) and second round multiplex PCR (A189f/A650r/mb661r): A189f (5'-GGNGACTGGGACTTCTGG-3'), A682r (5'-GAASGCNGAGAAGAASGC-3'), A650r (5'-ACGTCCTTACCGAAGGT-3'), mb661r (5'-CCGGMGCAACGTCYTTACC-3').

Sample	Target gene	Soil – file name	Barcode
B1-0	16S rRNA	fresh soil-bog- depth0cm-replicate-1	GTCACA
B2-0	16S rRNA	fresh soil-bog- depth0cm-replicate-2	TAGCAT
B3-0	16S rRNA	fresh soil-bog- depth0cm-replicate-3	ACGTAC
B4-0	16S rRNA	fresh soil-bog- depth0cm-replicate-4	TCAGAG
B1-5	16S rRNA	fresh soil-bog- depth5cm-replicate-1	AGCTGA
B2-5	16S rRNA	fresh soil-bog- depth5cm-replicate-2	CACAGT
B3-5	16S rRNA	fresh soil-bog- depth5cm-replicate-3	AGAGTC
B4-5	16S rRNA	fresh soil-bog- depth5cm-replicate-4	CGTATA
B1-10	16S rRNA	fresh soil-bog- depth10cm-replicate-1	AGTCAG
B2-10	16S rRNA	fresh soil-bog- depth10cm-replicate-2	CAGTCA
B3-10	16S rRNA	fresh soil-bog- depth10cm-replicate-3	AGCTGA
B4-10	16S rRNA	fresh soil-bog- depth10cm-replicate-4	GACTAG
B1-15	16S rRNA	fresh soil-bog- depth15cm-replicate-1	ATATCG
B2-15	16S rRNA	fresh soil-bog- depth15cm-replicate-2	CATGAC
B3-15	16S rRNA	fresh soil-bog- depth15cm-replicate-3	AGTCAG
B4-15	16S rRNA	fresh soil-bog- depth15cm-replicate-4	GAGATC
B1-20	16S rRNA	fresh soil-bog- depth20cm-replicate-1	ATCGAT
B2-20	16S rRNA	fresh soil-bog- depth20cm-replicate-2	CGATAT
B3-20	16S rRNA	fresh soil-bog- depth20cm-replicate-3	ATATCG
B4-20	16S rRNA	fresh soil-bog- depth20cm-replicate-4	GATCGA
B1-25	16S rRNA	fresh soil-bog- depth25cm-replicate-1	ATGCTA
B2-25	16S rRNA	fresh soil-bog- depth25cm-replicate-2	CGCGCG
B3-25	16S rRNA	fresh soil-bog- depth25cm-replicate-3	ATCGAT
B4-25	16S rRNA	fresh soil-bog- depth25cm-replicate-4	GTACAC
F1-0	16S rRNA	fresh soil-forest- depth0cm-replicate-1	TACGTA
F2-0	16S rRNA	fresh soil-forest- depth0cm-replicate-2	TATACG
F3-0	16S rRNA	fresh soil-forest- depth0cm-replicate-3	ACTGCA
F4-0	16S rRNA	fresh soil-forest- depth0cm-replicate-4	TCTCTC
F1-5	16S rRNA	fresh soil-forest- depth5cm-replicate-1	ACACGT
F2-5	16S rRNA	fresh soil-forest- depth5cm-replicate-2	AGTCAG
F3-5	16S rRNA	fresh soil-forest- depth5cm-replicate-3	CGTATA
F4-5	16S rRNA	fresh soil-forest- depth5cm-replicate-4	CAGTCA
F1-10	16S rRNA	fresh soil-forest- depth10cm-replicate-1	ACGTAC
F2-10	16S rRNA	fresh soil-forest- depth10cm-replicate-2	ATATCG
F3-10	16S rRNA	fresh soil-forest- depth10cm-replicate-3	GACTAG
F4-10	16S rRNA	fresh soil-forest- depth10cm-replicate-4	CATGAC
F1-15	16S rRNA	fresh soil-forest- depth15cm-replicate-1	ACTGCA
F2-15	16S rRNA	fresh soil-forest- depth15cm-replicate-2	ATCGAT
F3-15	16S rRNA	fresh soil-forest- depth15cm-replicate-3	GAGATC

F4-15	16S rRNA	fresh soil-forest- depth15cm-replicate-4	CGATAT
F1-20	16S rRNA	fresh soil-forest- depth20cm-replicate-1	AGAGTC
F2-20	16S rRNA	fresh soil-forest- depth20cm-replicate-2	ATGCTA
F3-20	16S rRNA	fresh soil-forest- depth20cm-replicate-3	GATCGA
F4-20	16S rRNA	fresh soil-forest- depth20cm-replicate-4	CGCGCG
F1-25	16S rRNA	fresh soil-forest- depth25cm-replicate-1	AGCTGA
F2-25	16S rRNA	fresh soil-forest- depth25cm-replicate-2	CACAGT
F3-25	16S rRNA	fresh soil-forest- depth25cm-replicate-3	GTACAC
G1-0	16S rRNA	fresh soil-grass- depth0cm-replicate-1	GTGTGT
G2-0	16S rRNA	fresh soil-grass- depth0cm-replicate-2	GTGTGT
G3-0	16S rRNA	fresh soil-grass- depth0cm-replicate-3	ATGCTA
G4-0	16S rRNA	fresh soil-grass- depth0cm-replicate-4	TCGAGA
G1-5	16S rRNA	fresh soil-grass- depth5cm-replicate-1	GACTAG
G2-5	16S rRNA	fresh soil-grass- depth5cm-replicate-2	TACGTA
G3-5	16S rRNA	fresh soil-grass- depth5cm-replicate-3	CACAGT
G4-5	16S rRNA	fresh soil-grass- depth5cm-replicate-4	TCTCTC
G1-10	16S rRNA	fresh soil-grass- depth10cm-replicate-1	GAGATC
G2-10	16S rRNA	fresh soil-grass- depth10cm-replicate-2	TAGCAT
G3-10	16S rRNA	fresh soil-grass- depth10cm-replicate-3	CAGTCA
G4-10	16S rRNA	fresh soil-grass- depth10cm-replicate-4	ACACGT
G1-15	16S rRNA	fresh soil-grass- depth15cm-replicate-1	GATCGA
G2-15	16S rRNA	fresh soil-grass- depth15cm-replicate-2	TATACG
G3-15	16S rRNA	fresh soil-grass- depth15cm-replicate-3	CATGAC
G4-15	16S rRNA	fresh soil-grass- depth15cm-replicate-4	ACGTAC
G1-20	16S rRNA	fresh soil-grass- depth20cm-replicate-1	GTACAC
G2-20	16S rRNA	fresh soil-grass- depth20cm-replicate-2	TCAGAG
G3-20	16S rRNA	fresh soil-grass- depth20cm-replicate-3	CGATAT
G4-20	16S rRNA	fresh soil-grass- depth20cm-replicate-4	ACTGCA
G1-25	16S rRNA	fresh soil-grass- depth25cm-replicate-1	GTCACA
G2-25	16S rRNA	fresh soil-grass- depth25cm-replicate-2	TCGAGA
G3-25	16S rRNA	fresh soil-grass- depth25cm-replicate-3	CGCGCG
G4-25	16S rRNA	fresh soil-grass- depth25cm-replicate-4	AGAGTC
pmoA-B1-0	*pmoA*	fresh soil-bog- depth0cm-replicate-1	CACAGT
pmoA-B2-0	*pmoA*	fresh soil-bog- depth0cm-replicate-2	GACTAG
pmoA-B3-0	*pmoA*	fresh soil-bog- depth0cm-replicate-3	TACGTA
pmoA-B1-5	*pmoA*	fresh soil-bog- depth5cm-replicate-1	CAGTCA
pmoA-B2-5	*pmoA*	fresh soil-bog- depth5cm-replicate-2	GAGATC
pmoA-B3-5	*pmoA*	fresh soil-bog- depth5cm-replicate-3	TAGCAT
pmoA-B1-10	*pmoA*	fresh soil-bog- depth10cm-replicate-1	CATGAC
pmoA-B2-10	*pmoA*	fresh soil-bog- depth10cm-replicate-2	GATCGA
pmoA-B3-10	*pmoA*	fresh soil-bog- depth10cm-replicate-3	TATACG
pmoA-B1-15	*pmoA*	fresh soil-bog- depth15cm-replicate-1	CGATAT
pmoA-B2-15	*pmoA*	fresh soil-bog- depth15cm-replicate-2	GTACAC
pmoA-B3-15	*pmoA*	fresh soil-bog- depth15cm-replicate-3	TCAGAG
pmoA-B1-20	*pmoA*	fresh soil-bog- depth20cm-replicate-1	CGCGCG
pmoA-B2-20	*pmoA*	fresh soil-bog- depth20cm-replicate-2	GTCACA
pmoA-B3-20	*pmoA*	fresh soil-bog- depth20cm-replicate-3	TCGAGA
pmoA-B1-25	*pmoA*	fresh soil-bog- depth25cm-replicate-1	CGTATA
pmoA-B2-25	*pmoA*	fresh soil-bog- depth25cm-replicate-2	GTGTGT

pmoA-B3-25	*pmoA*	fresh soil-bog- depth25cm-replicate-3	TCTCTC
pmoA-F1-0	*pmoA*	fresh soil-forest- depth0cm-replicate-1	ACACGT
pmoA-F2-0	*pmoA*	fresh soil-forest- depth0cm-replicate-2	ATATCG
pmoA-F3-0	*pmoA*	fresh soil-forest- depth0cm-replicate-3	CGATAT
pmoA-F1-5	*pmoA*	fresh soil-forest- depth5cm-replicate-1	ACGTAC
pmoA-F2-5	*pmoA*	fresh soil-forest- depth5cm-replicate-2	ATCGAT
pmoA-F3-5	*pmoA*	fresh soil-forest- depth5cm-replicate-3	CGCGCG
pmoA-F1-10	*pmoA*	fresh soil-forest- depth10cm-replicate-1	ACTGCA
pmoA-F2-10	*pmoA*	fresh soil-forest- depth10cm-replicate-2	ATGCTA
pmoA-F3-10	*pmoA*	fresh soil-forest- depth10cm-replicate-3	CGTATA
pmoA-F1-15	*pmoA*	fresh soil-forest- depth15cm-replicate-1	AGAGTC
pmoA-F2-15	*pmoA*	fresh soil-forest- depth15cm-replicate-2	CACAGT
pmoA-F3-15	*pmoA*	fresh soil-forest- depth15cm-replicate-3	GACTAG
pmoA-F1-20	*pmoA*	fresh soil-forest- depth20cm-replicate-1	AGCTGA
pmoA-F2-20	*pmoA*	fresh soil-forest- depth20cm-replicate-2	CAGTCA
pmoA-F3-20	*pmoA*	fresh soil-forest- depth20cm-replicate-3	GAGATC
pmoA-F1-25	*pmoA*	fresh soil-forest- depth25cm-replicate-1	AGTCAG
pmoA-F2-25	*pmoA*	fresh soil-forest- depth25cm-replicate-2	CATGAC
pmoA-F3-25	*pmoA*	fresh soil-forest- depth25cm-replicate-3	GATCGA
pmoA-G1-0	*pmoA*	fresh soil-grass- depth0cm-replicate-1	GTACAC
pmoA-G2-0	*pmoA*	fresh soil-grass- depth0cm-replicate-2	TCAGAG
pmoA-G3-0	*pmoA*	fresh soil-grass- depth0cm-replicate-3	AGAGTC
pmoA-G1-5	*pmoA*	fresh soil-grass- depth5cm-replicate-1	GTCACA
pmoA-G2-5	*pmoA*	fresh soil-grass- depth5cm-replicate-2	TCGAGA
pmoA-G3-5	*pmoA*	fresh soil-grass- depth5cm-replicate-3	AGCTGA
pmoA-G1-10	*pmoA*	fresh soil-grass- depth10cm-replicate-1	GTGTGT
pmoA-G2-10	*pmoA*	fresh soil-grass- depth10cm-replicate-2	TCTCTC
pmoA-G3-10	*pmoA*	fresh soil-grass- depth10cm-replicate-3	AGTCAG
pmoA-G1-15	*pmoA*	fresh soil-grass- depth15cm-replicate-1	TACGTA
pmoA-G2-15	*pmoA*	fresh soil-grass- depth15cm-replicate-2	ACACGT
pmoA-G3-15	*pmoA*	fresh soil-grass- depth15cm-replicate-3	ATATCG
pmoA-G1-20	*pmoA*	fresh soil-grass- depth20cm-replicate-1	TAGCAT
pmoA-G2-20	*pmoA*	fresh soil-grass- depth20cm-replicate-2	ACGTAC
pmoA-G3-20	*pmoA*	fresh soil-grass- depth20cm-replicate-3	ATCGAT
pmoA-G1-25	*pmoA*	fresh soil-grass- depth25cm-replicate-1	TATACG
pmoA-G2-25	*pmoA*	fresh soil-grass- depth25cm-replicate-2	ACTGCA
pmoA-G3-25	*pmoA*	fresh soil-grass- depth25cm-replicate-3	ATGCTA

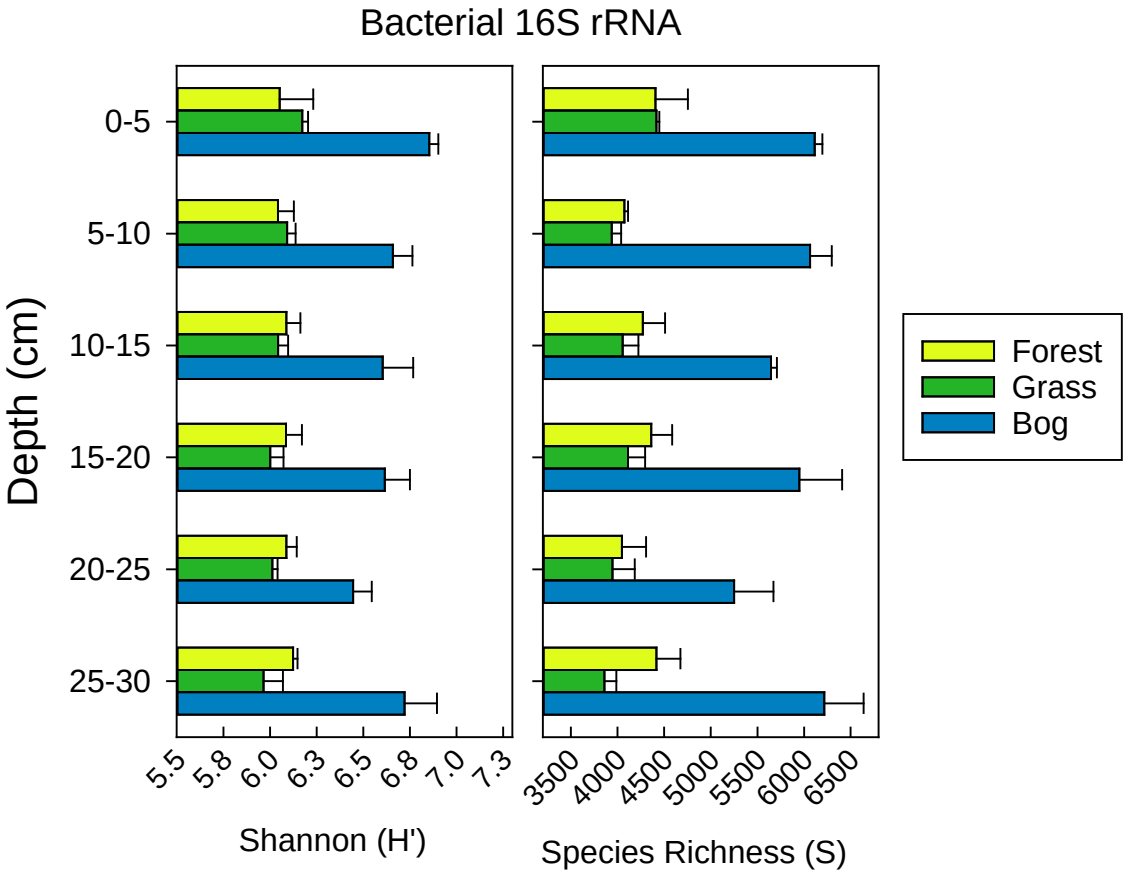

Figure S1. Bacterial 16S rRNA gene diversity measured as Shannon Diversity (H') and Richness (S) (n=4, means ± standard errors).

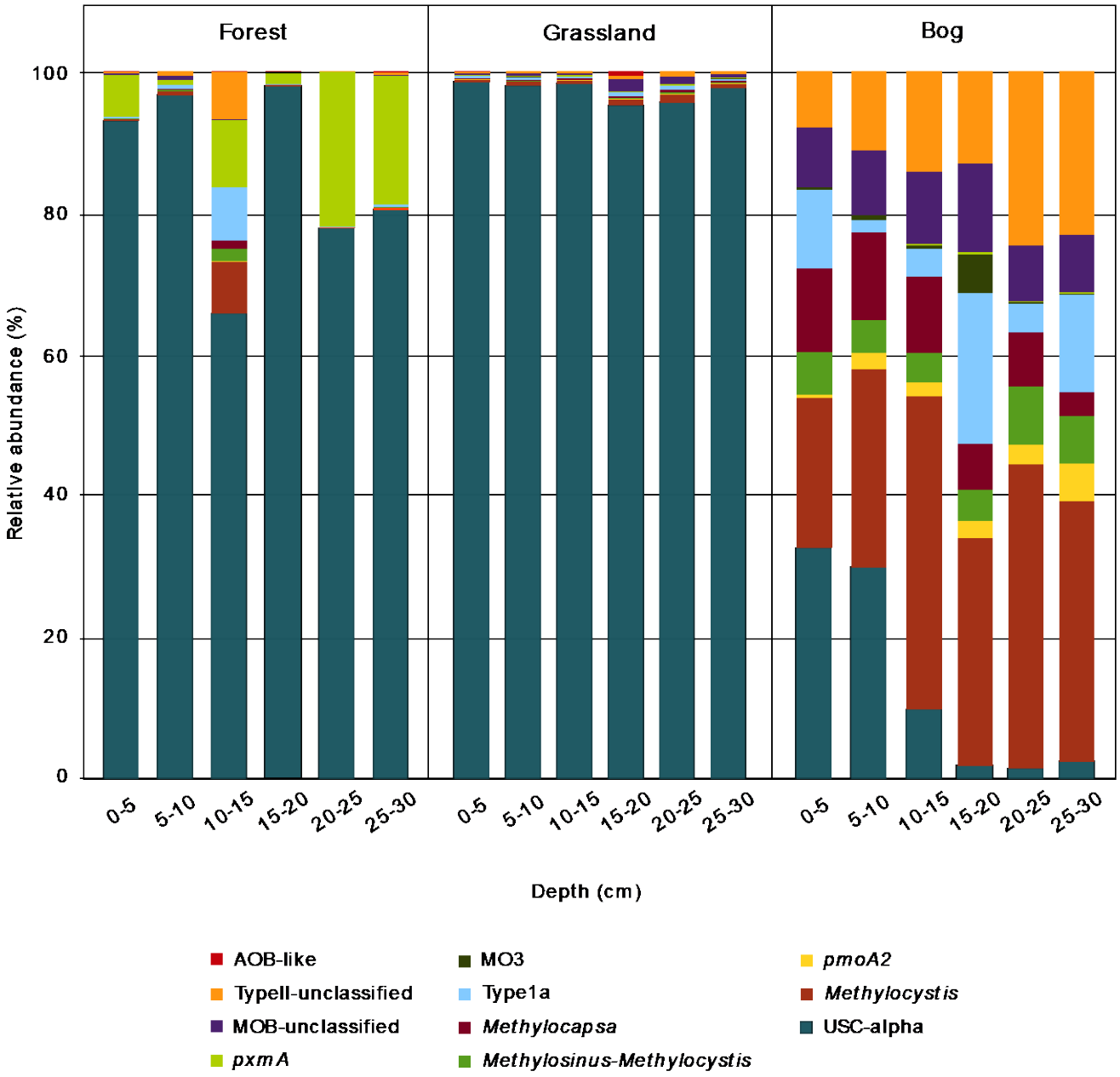

Figure S2. Relative abundance of *pmoA* genes of the dominant methanotroph groups.

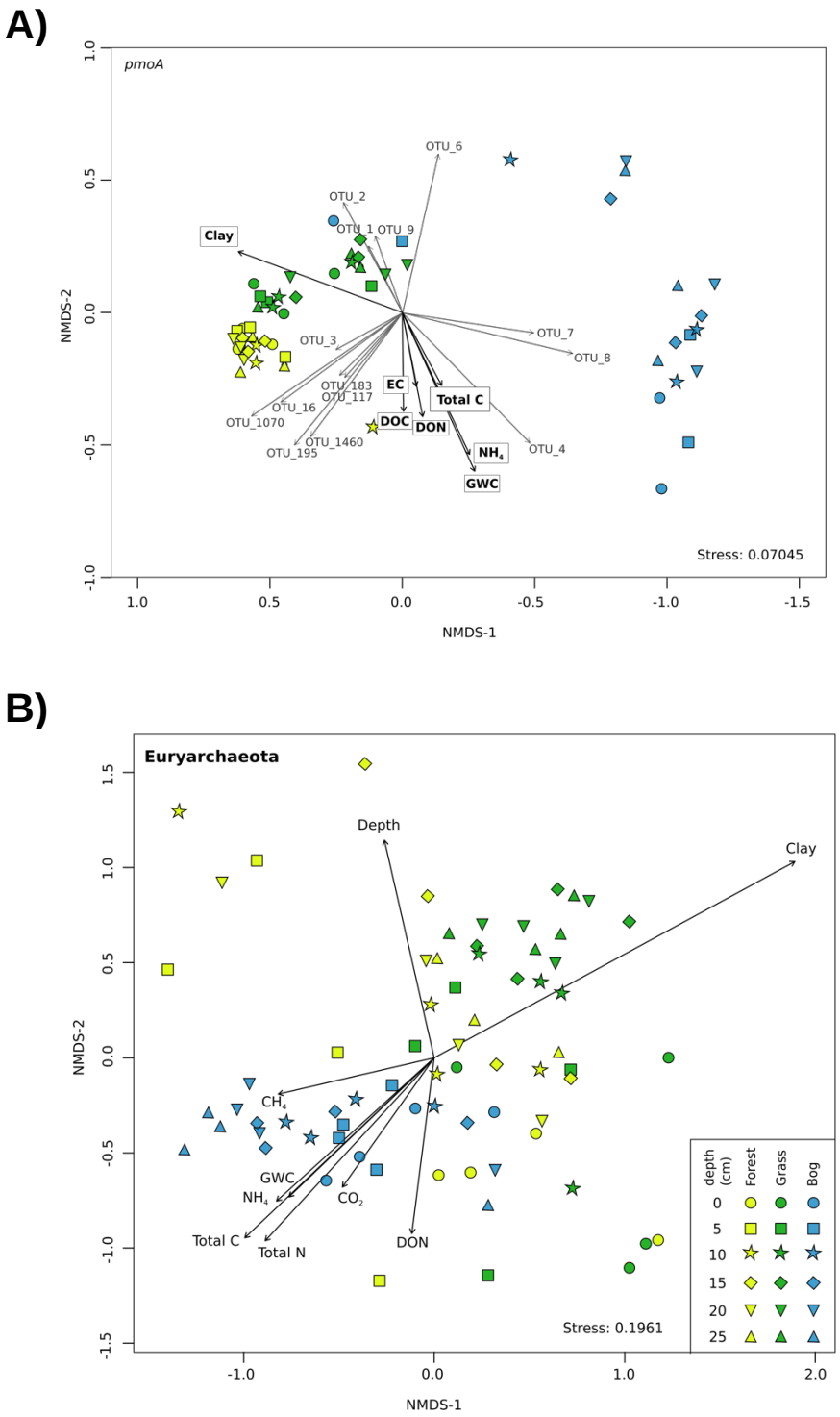

Figure S3. NMDS ordination of *pmoA* (A) and euryarchaeota (B) communities based on the Bray–Curtis dissimilarity of community composition. Shape indicates depth and sites are colored according to the soil typel. The arrows indicate the direction at which the environmental vectors fit the best (using the *envfit* function) onto the NMDS ordination space. Abbreviations: DOC, dissolved organic carbon; DON, dissolved organic nitrogen; EC, electrical conductivity; GWC, gravimetric water content; NH_4, ammonium.

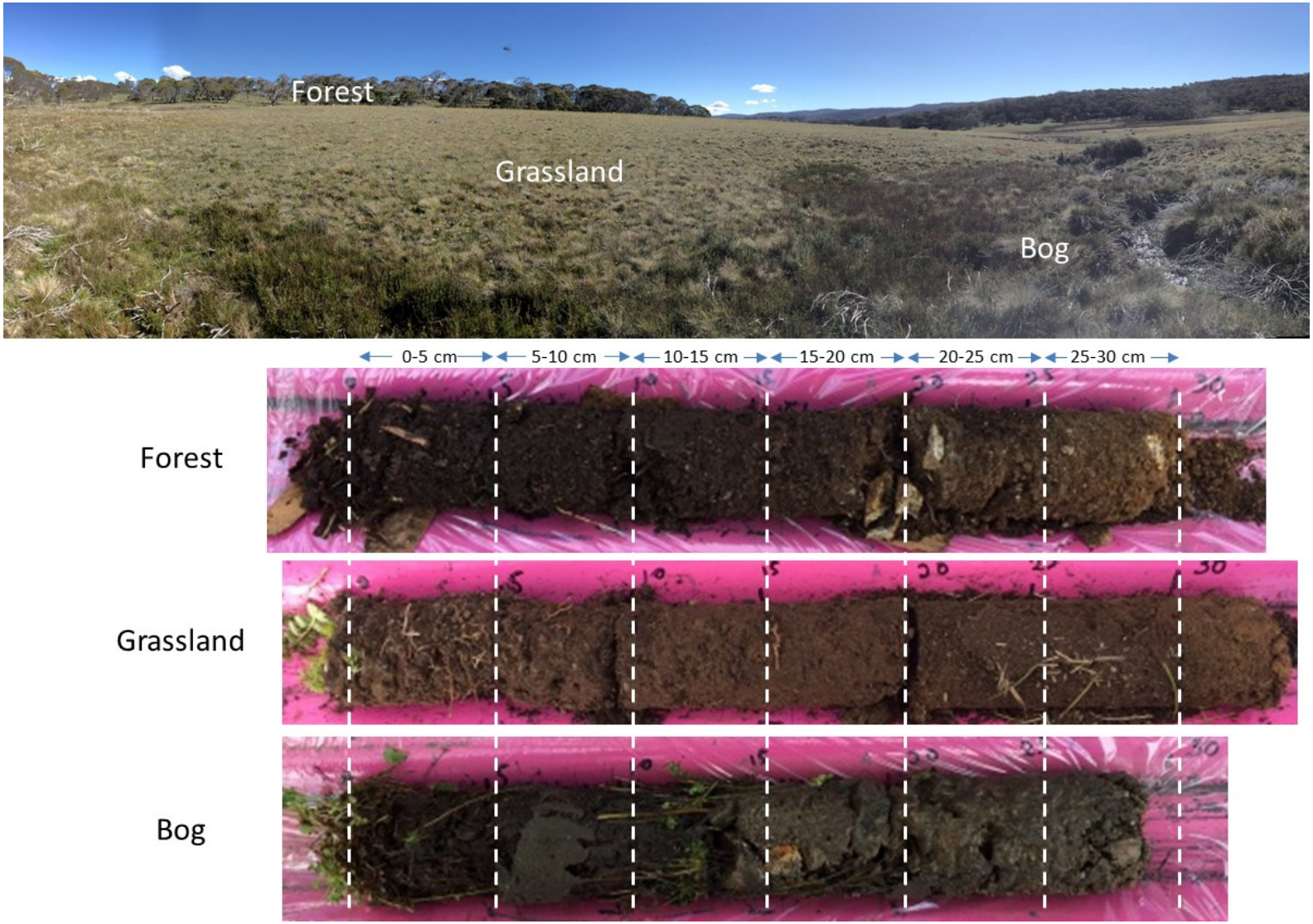

Figure S4. Soil/Vegetation gradient (Forest-Grassland-Bog) located in Snowy Mountains region near Kosciuszko National Park, NSW, Australia. Soil/vegetation types shown above, below are three soil cores from each of the soil/vegetation types.